IEPC-93-034

# PERFORMANCE ESTIMATE OF LARGE-SCALE ION ENGINES FOR SEI-TYPE MISSIONS USING $C_{60}$ PROPELLANT

Juergen Mueller*

*Jet Propulsion Laboratory*
*California institute of Technology*
*Pasadena, CA 91109*

A performance estimate of large scale ion engines intended for use on missions of the type envisioned by the Space Exploration Initiative (SEI) has been conducted. $C_{60}$, xenon, krypton and argon propellants were compared. Thruster diameters between SO cm and 100 cm were examined analytically. Engine performance parameters, such as thrust, efficiency, specific mass, thruster input power, thrust-to-power ratio and discharge current have been calculated with specific impulse the independent variable. Thrust-to-power ratios for $C_{60}$ propellant were predicted to be as more than twice the values obtainable for xenon. Thrust values up to 4 N are predicted for a 1-m engine at 80 kW for $C_{60}$ and 200 kW for xenon. Significantly higher power levels are required for the other inert gases. For a maximum span-to-gap ratio of 500, a maximum accelerating voltage of 6 kV and a maximum net-to-total voltage ratio of 0.9, $C_{60}$ thrusters are theoretically able to obtain specific impulse values up to 3000 see, while xenon, krypton and argon maybe able to deliver 7500 see, 9500 sec and 12,000 see) respectively.

## NOMENCLATURE

| | |
|---|---|
| $A_B$ | = Beam Area |
| $D_g$ | = Grid Diameter |
| $d_s$ | = Screen Grid Hole Diameter |
| e | = Unit Electric Charge (1 .602 x 10-16 As) |
| $E_m$ | = Maximum Electric Field Strength |
| $f_B$ | = Beam Flatness Parameter |
| g | = Gravitational Acceleration |
| $I_B$ | = Beam Current |
| $I_D$ | = Discharge Current |
| $I_{sp}$ | = Specific Impulse |
| j | = Average Current density |
| $j_{max}$ | = Maximum Current Density |
| $l_e$ | = Effective Acceleration Length |
| $l_g$ | = Grid Spacing |
| $\dot{m}$ | = Propellant Flow Rate |
| $m_i$ | = Ion Mass |
| $M_W$ | = Molar Weight |
| NPPH | = Normalized Perveance Parameter |
| $P_I$ | = Thruster Input Power |
| $P_{Heat}$ | = Heater Power |
| $P_S$ | = Sublimation Power |
| R | = Net-to-Total Voltage Ratio |
| [s/g] | = Span-to-Gap Ratio |
| T | = Thrust |
| [T/P] | = Thrust-to-Power Ratio |
| $V_B$ | = Beam Voltage |
| $V_{NC}$ | = Neutralizer Coupling Voltage |
| $V_T$ | = Total Accelerating Voltage |
| $\alpha$ | = Specific Mass |
| $\delta$ | = Thrust Divergence 1 .0ss Factor |
| $\Delta H_S$ | = Heat of Sublimation |
| $\eta_{el}$ | = Electric Efficiency |
| $\eta_{Heat}$ | = Heatr Efficiency |
| $\eta_T$ | = Thruster Efficiency |
| $\Phi_S$ | = Open Area Fraction |

* Member of Technical Staff, Advanced Propulsion Technology Group, Member AIAA

## INTRODUCTION

### Motivation for this Study:

Missions of human exploration to the moon and Mars have always been of keen interest, Missions of this kind, until the very recent past, have been studied under the so called "Space Exploration Initiative" ("SEI"). Large projected costs, however, have raised questions whether development efforts required for such missions to take place early in the next century can be accomplished within the current budgetary situation of the major industrial nations. Onc important cost factor for all space missions, and in particular large-scale SEI-type missions, arc launch costs from Earth's surface into I .ow Earth Orbit (1 .EO). These costs arc largely determined by the mass to be inserted in(o LEO. Studies have shown that in particular for large scale robotic. and human Mars missions requiribg the delivery of payloads on the order of 100 metric tons (MT) to Mars, initial masse.s in LEO (IMLEO) can be enormous if conventional, chemical (1 .H/LOX) systems arc being used for the LEO 10 Mars transfer[1-4]. For a 100 MT payload, IMLEO's of over 400 MI' can be expected for an LH/LOX system[2], increasing to roughly 1 S00 M']' if a payload of about 400 MT (delivery only) were to be transported to our neighbor planet[1]. 1 ligh IMLEO's also have to be expected for a chemical vehicle transporting a significantly lower payload mass if part of the payload is to be returned to Earth orbit; such a scenario would be typical for a manned mission. For a 137 Ml' Mars-bound payload and a 61 M-I' Earth-bound payload, Braun and Blersch[3] determined IMLEO masses between 1000 and up to 5000 MT (depending On the launch date) for a total round trip time of 1 to 2 years using a Venus swing-by.

Because of these high departure masses out of 1 .EO for chemical propulsion systems, other, more advanced propulsive options have been considered for SEI-type missions. Among the concepts arc nuclear-thermal (NTP) and nuclear-electric (NEP) or solar -electric (SEP) propulsion systems. In NTP systems the propellant, typically hydrogen gas, is heated by conduction from the reactor core and then expanded thermally in a conventional nozzle. Specific impulses of 825 scc have been obtained in the NERVA (Nuclear Engine for Rocket Vehicle Application) program in the late 60's and early 70's[1]. Although trip lime reductions using an NTP vehicle (o Mars can be significant compared to chemical vehicles (typically 50% reduction in flight time), IMLEO mass savings arc more moderate. Depending on payload mass, IMLEO mass reductions arc only on the order of 10%[2].

NEP systems, on the other hand, have shown IMLEO mass reductions around 50%[1,3,4] using a combination of nuclear-generated electric power and ion thrusters for the propulsion system, The actual value for the IMLEO mass reduction depends heavily on such parameters as the specific mass of the power plant and propulsion system, power output of the onboard power source as well as restrictions regarding flight time. Currently, ion engines arc the only electric propulsion systems that have reached a degree of maturity and performance high enough for usc on interplanetary missions. However, they deliver only relatively low thrust values. The reason for this can be found in the space charge limitation of the ion beam, allowing only a certain maximum ion current to be extracted for a given thruster diameter, grid spacing and accelerator voltage[5,6]. Since thrust for an ion engine is proportional to the beam current, thrust values will be limited. Low thrust values will result in long trip times unless large amounts of onboard power is available that can be coupled into a large nurnber of thrusters. Therefore, if trip times shorter than those obtainable with chemical systems arc desired, the IMLEO mass of NEP systems can raise dramatically[1].

One way to increase thrust for a given power level or specific impulse is to usc heavy ion propellants. In the past, however, problems have arisen using large molecular propellants duc to fragmentation of these molecules. Fragmentation was found to be duc to ioni?.alien, excitation and thermal dissociation. Recently, however, Leifer et al.[8] suggested a new heavy molecular propellant for ion propulsion applications, a carbon cluster consisting of 60 carbon atoms - $C_{60}$. The $C_{60}$ molecule is shown in Fig. 1 and exhibits certain interesting properties such as high molecular mass (720 amu), low ionization potential ( 7.6 cV) and high stability against fragmentation.

Leifer c1 al. investigated potential performance benefits of $C_{60}$ ion propulsion systems over conventional (i.e. xenon) ion thrusters for engines in the 5 kW electric power and 30 cm thruster diameter range as applicable for near-earth orbit transfer missions[8]. Results for $C_{60}$ were obtained using analytical expressions for thruster efficiency and ion beam production costs[8]. These expressions were dc.rived from an ion thruster performance model developed by Brophy[9]. It was found that $C_{60}$ ion thrusters arc projected to outperform xenon ion thrusters of the same size with respect to thruster efficiency[8]. In the lower specific impulse range of 1000-2000 sec, being of particular importance for orbit transfer missions, thruster efficiencies for the $C_{60}$ thruster arc projected to be as high as 80% compared to efficiencies of only 50% and lower for xenon engines. Higher thruster efficiencies will allow for a more economical usage of tbc provided onboard power and thus enable power system mass reductions or shorter trip times.

The higher mass of the propellant was identified as a major driver for this performance increase of $C_{60}$ engines[8]. In an ion engine, power is consumed during the. generation of ions, the electrostatic acceleration of these ions and smaller amounts during beam neutralization. Apart from smal 1 beam d ivergence lo sscs, the process of ion acceleration is very efficient, much more so than the process of ion generation with its significant ion and electron wall losses as well as excitation losses. In an ion engine. using heavy ions, a much larger portion of the energy per unit mass is expended on the. acceleration of the heavier ions than on ion generation. Therefore, overall thruster efficiency can potentially be significantly higher for a heavy-parliclc ion engine,

This expected high thruster efficiency and thrust-to-power ratio of a $C_{60}$ ion engine motivated the investigation of the applicability of $C_{60}$ ion thrusters for SEI missions. Higher thrust values and thus lower trip times are of particular importance for piloted Mars missions, reducing the exposure of the crew to harmful solar radiation. Although optimal specific impulse ranges for SEI-type missions using inert gas ion thrusters are usually quoted at value.s significantly higher than those favored by $C_{60}$ ion thrusters[1], this dots, not necessarily preclude the usc of $C_{60}$ engines for this type of missions. The optimum specific impulse, although mainly mission driven, will be affected by the propellant type and its efficiency vs. specific impulse characteristics, which may yield a different optimum specific impulse when $C_{60}$ thrusters were used. It is the purpose of this study to estimate these performance characteristics. Although the. primary application for a $C_{60}$ ion thruster will most likely be found in near-carlhorbil transfer missions because of its potential high performance in those relatively low specific impulse ranges, the identification of potential performance benefits that may be obtained with $C_{60}$ thrusters compared to more conventional inert gas thrusters in a performance range applicable to SEI-type missions could serve as an additional incentive for the development of this engine type.

## Scope and Relevance of this Study:

The purpose of this study was to take a "first look" at the, idea of using $C_{60}$ ion thrusters for large scale lunar and interplanetary missions. As a first step toward this goal, an attempt was made to estimate the. performance characteristics of large scale $C_{60}$ ion engines using an analytical model. Comparative calculations were performed for large scale ion thrusters using inert gas propellants, such as xenon, krypton and argon. The.se performance cst imates were focused on a study of large scale ion engine. technology only in order to satisfy a corresponding need by mission planners in this regard. It was beyond the scope of this study to conduct an investigation of SIil-type mission scenarios. However, the data base obtained in this study may be applied by mission designers for large scale lunar or interplanetary mission planning in a second step,

This investigation has been part of a larger research effort to identify new and unique electric propulsion systems that may Offer performance benefits over current technology[10]. This study is structured into two major parts. In the first part, a rc.view of the state-of-the-arl of $C_{60}$ ion propulsion research is presented. Since $C_{60}$ is still relatively unknown within the propulsion community, a background on the brief history of $C_{60}$ and some of its unique properties is given and current activities in $C_{60}$ ion engine testing are summarized. The purpose of such a summary is to draw attention to some feasibility issues of this engine concept which can not be properly accounted for in the analytical model. In the second part, an analytical model used to estimate large scale $C_{60}$ thruster performances is presented. This model is based on an earlier analysis performed by Leifer et al.[11] with only minor changes added. Performance characteristics for $C_{60}$ thrusters were estimated using this model and compared with those, obtained for the inert gas propellants argon, krypton and xenon. Emphasis was placed on the prediction of key performance parameters, such as efficiency, power consumption, thrust, mass and specific mass, over a wide range of operating conditions, thus offering the mission dc.signer flexibility in exploring a variety of mission profiles.

Given the early, concept-stage development status of $C_{60}$ ion engine technology such an investigation may seem premature. However, propulsion will play a key role in reducing overall spacecraft mass and, thus, costs for SEI-type missions. Furthermore, the fact that cost considerations will strongly impact the decision on whether or not to proceed with SfO-type missions or not, a study on bow new propulsion systems, such as $C_{60}$ ion engines, may benefit those missions seems warranted. Mission planners intending to usc data obtained in this study, however, should recognize that substantial development efforts to arrive at an actually working $C_{60}$ ion thruster are still required. Rc.suits obtained from future $C_{60}$ engine testing will most certainly force a revision of this study and likely change some of the obtained results. Therefore, this study has to be viewed as an approximate performance characterization of this engine. cone.till,

This study was conducted in late spring of 1992. Significant changes have occurred in the US space. program since then. At the time of this writing, tbc NASA Office of Exploration, that has conducted and overseen SEI mission studies, has been shut down and remaining SEI related activities will be performed within the newly created Office of Space. Science, de-emphasizing the Space Exploration Initiative[12,13]. As a consequence of scaled-back plans for missions of human exploration, research and development on the S1'- 100 space nuclear reactor program has been halted[14], endangering nuclear-electric mission proposals. However, it is expected that studies of human missions to the Moon and Mars will continue on a smaller scale and it is hoped that data obtained in this investigation may serve as a source of reference for future study efforts in this area.

## STATE-OF-THE-ART OF $C_{60}$ ION ENGINE RESEARCH

### Background:

Due to recent, rapid developments in the field of carbon cluster physics, it seems useful to briefly review some of the characteristics and properties of this unique molecule. $C_{60}$ was first discovered by Rohlfing et al.[15] in 1984 as part of an entire "family" of pure carbon clusters, ranging in size from individual carbon atoms to clusters containing up to 190 atoms. These clusters were. generated by evaporating a solid graphite rod with a laser in a helium flow to cool the clusters after formation and, afterwards, expanding the resulting molecular beam through a supersonic nozzle[15]. Interestingly, this early research on carbon clusters was stimulated by astrophysical research and the problem of identifying certain absorption bands in the optical spectra of red giant stars and comet tails that had defied explanation for over 70 years[15-18]. Carbon cluster nucleation experiments were aimed at simulating the conditions under which these clusters might form in space[17] Although in the end it was found that spectra obtained under laboratory conditions did not seem to match those astronomical data [16,18] a flurry of research in carbon cluster physics was initiated by those early experiments.

initial research was focused on a basic understanding of the obtained clustering results. Rohlfing et al. [15] and soon thereafter Smalley and Kroto et al. [19] and Smalley et al.[20] noticed several peculiar characteristics in the mass spectra obtained for these carbon clusters. It was noted that mass spectra seemed to be divided into two different portions, with the $C_{32}$ cluster marking the dividing line.. For larger clusters, only cluster sizes with an even number of carbon atoms could be observed[15,19,20], while for clusters with less than 32 atoms even and odd clusters were found, with intensity maxima obtained for clusters $C_n$ with n= 11,15,19,23 and 27 and minima for n= 13, 17,25 and 29[15]. For clusters larger than n=32, a strong peak was found for $C_{60}$[15,17-20] with up to more than 50% of the larger cluster mass accounted for by this cluster alone, depending on experimental conditions[19]. Other dominant peaks, although smaller than the one obtained for $C_{60}$ were noted for $C_{70}$ as well as $C_{50}$[15,17-20]. These findings seemed to indicate a particular stability of these clusters compared to others, Clusters with sizes around the $C_{32}$ cluster were markedly absent in the mass spectra[15,17-20].

Photofragmentation studies by Smalley et al.[20,21] and Weiss et al.[22] were aimed at further investigating the various degrees of stability found for the different carbon clusters. It was found upon last.r irradiation that carbon clusters smaller than the $C_{32}$ cluster fragment by loss of $C_3$, which is known to be a very stable fragnlent[21]. Clusters larger than $C_{32}$, however, fragmented by loosing $C_2$, which was surprising since this fragment is known to be less stable than $C_3$[21], However, loss of $C_2$ fragments by an even cluster will allow for formation of only even daughter fragments, a fact that appears to play a key role in cluster formation and cluster stability for the larger type clusters. During all photofragmentation studies of very large clusters it was noted furthermore that $C_{60}$ and $C_{70}$ as well as $C_{50}$ daughter fragments were favored and that further fragmentation of these clusters and their ions was extremely difficult at the laser fluxes employed throughout the expcrinlents[20-23]. This fact seems to underline again the extraordinary stability of these clusters, with $C_{60}$ found to be the most stable of all. The C32 cluster itself was found not to obey either one of the two fragmentation rules mentioned above and completely shattered upon irradiation into fragments in the 10-19 atom range[21], explaining the absence of clusters in this portion of the mass spectrum.

Observations like these have led Smalley et al, [19] to suggest the possible structure for the $C_{60}$ cluster depicted in Fig. 1. The molecule basically takes on the. shape of a soccer ball with carbon atoms placed on each vertex of the seams of the ball. Because of the similarity of this structure to the one of the geodesic domes of the architect Buckminster Fuller, Smalley et al, [19] subsequently name.d the $C_{60}$ molecule "*buckminsterfullerene*". The carbon atoms are arranged in forms of hexagons and pentagons throughout the mole.cule as shown in Fig. 1, connected by single and double bonds, respectively, with no two pentagons adjacent to each other[24]. This arrangement places the carbon atoms onto a icosahedron with respect to each other. The diameter of the $C_{60}$ molecule has been determined to 7. I A] [6-18]. Interestingly, it can be shown theoretically that exactly 12 pentagons are required for an otherwise graphitic (i.e. hexagonal) sheet to curve into a closed shell such as $C_{60}$, independent of its actual size[24]. Later on[20] it was suggested that all large clusters have a similar shell structure, with $C_{70}$ appearing slightly oblate and higher order clusters developing "cusps" in their structure at the locations of the. twelve pentagons. Strains in the molecular structure expected to focus in these regions 17 could make these clusters more susceptible to fragmentation than $C_{60}$, where. strains arc distributed evenly throughout the molecule. The entire "family" of large, closed shell carbon clusters was subsequently named "*fullerenes*" after the buckminsterfu llerene $C_{60}$ structure which they resemble. Smaller clusters, on the other hand, were visual ized as predominantly onc and two-din~cnsiona1 [20*2]1 with many "dangling", free bonds. This feature would explain the observed high reactivity of small carbon clusters versus the chemical inertness of large carbon clusters, even when the latter were exposed to such gases as 02, NH 3, NO, CO, and S02[17,21]. Air oxidation of $C_{60}$ was only noted above 400°C[25]. Also explained by this model would be the fact that only even numbered large clusters exist. Although odd cluster shells arc allowed to form, they would have several free carbon bonds which enable these clusters to react to form more stable cl usters[20].

Although Smalley's model was able to explain several of the characteristics of carbon clusters mentioned above, skepticism initially prevailed on how such complicated molecular structures could form in condensing carbon vapor[17,21]. 11 has been suggested that large carbon clusters arc formed initially by individual carbon atoms or very small clusters present in the vapor, rather than "graphitic sheds" broken of the solid graphite sample during vapor ization[17]. The latter conclusion seems to be confirmed by the fact that fullerenes cannel only be produced by vaporizing graphite, but also from the condensing carbon vapor of diamond[17] and coal[26]. Small clusters with their large amount of free bonds arc able to react and form subsequentl y larger clusters. 1 f pentagonal shaped structures arc integrated in lo a graphitic, hexagonal shaped carbon bond, the. graphitic sheet curls. If exactly 12 pentagons arc present in the right locations in an otherwise hexagonal structure, the sheet may close up on itself and a fullerene is created [17,21,24]. However, duc to imperfections in the carbon structure, most clusters will not close upon themselves but form nau[ilus-like shells, i.e. the leading edge of the forming cluster shell "overshoots" the trailing edge and the shell will be unable to close[17,21,24]. Such nautilus shells will have many free bonds which will allow them to react and form more stable clusters. The relatively inert closed shells without any free bonds, however, arc left behind in this nucleation process and arc consequently detected in the carbon vapor. It should be noted, however, that the carbon vapor nucleation process is not fully understood yet and that the scenario given above might have to bc revised[27].

Probably the next important step in carbon cluster physics after the discovery of fullerenes and the identification of their structure, was a modified method of fullerene production demonstrated by Krätschmer et al. [18]. This method allowed for the production of macroscopic quantities of $C_{60}$ and other carbon clusters, rather than the microscopic quantities produced by the laser vaporization experiments discussed earlier. in Krätschmer's method[18], carbon vapor is produced by resistive heating of two graphite electrodes touching each other. Currents fed into the graphite electrodes arc on the order of 100 amps and both AC and DC currents have been used[16]. Since the graphite rods arc being consumed in the vaporization process, they have to bc continuously fed into the reaction chamber, The graphite vaporization process is performed in a pure helium environment at roughly 200 Torr (266,64 kPa) pressure. Yields of $C_{60}$ for this method have been found to vary greatly with helium pressure[16]. Some researchers believe that helium aids in the cluster nucleation process by keeping the forming carbon clusters c1osc to the heated graphite electrodes, thus allowing them to form larger clusters[28]. The carbon vapor finally condenses as soot on collecting surfaces. The soot is scraped of these surfaces and dispersed in either benzene or toluene. $C_{60}$, $C_{70}$ as well as traces of larger fullerenes go into solution and arc thus separated from the remainder of the soot. Evaporat i ng the. benzene or toluene leaves a crystalline powder consisting of $C_{60}$, $C_{70}$ and traces of larger fullerenes. Krätschmer el al. [18] called lhis solid "*fullerite*". $C_{60}$ *is* clearly dominant in fullerite and depending on the manufacturing procedure can bc found in ratios of $C_{60}/C_{70}$ of up 10510117. The ability 10 produce macroscopic quantities of $C_{60}$ is obviously of importance for its potential application as an electric rocket propellant as well and will be discussed in greater detail further below.

The fullerite was shown to consist of crystals, shaped in forms of rods, platelets and star-like flakes* 8. Further investigation *$17 indicated that the $C_{60}$ cluster retains its shape even in the solid phase and that the crystals consists of an array of $C_{60}$ cl usters, separated by about 3 Å (1 0Å center-to-center) and bonded by relatively strong van-der-Waals forces, At room temperature, the carbon clusters rotate in their positions within the lattice[17]. Solid $C_{60}$ has a density[16] of 1.7 g/cm$^3$ and sublimate.s directly into the gas phase at temperatures between 300-400°C [16-18]. Solid $C_{60}$ is a semiconductor, i.e. non-conducting unless it is doped. Foreign atoms placed between the $C_{60}$ molecules in the lattice can make the new compound superconductive[16,28-30]. Table 1 summarizes some of the $C_{60}$ properties discussed in this section.

Because of the ability to produce macroscopic quantities of predominantly $C_{60}$ and $C_{70}$ carbon clusters and since it became quite obvious during earlier experiments that these clusters were surprisingly stable, a significant amount of research was subsequently focused on these two fullerenes. Young et al.[31] conducted a collisional study of $C_{60}$ and $C_{70}$ ions with oxygen and helium as collision gases. Once again a preference for the formation of $C_{60}$ and to a smaller extend $C_{50}$ daughter fragments was noted upon fragmentation of $C_{70}$, underlining

'J'able. 1: Some I'roper-iics of Solid $C_{60}$

| Properties of Solid $C_{60}$ | |
|---|---|
| Density | 1.7 g/cm$^3$ |
| Molecule Mass | 720 AMU |
| Ionization Potential | 7.61 eV |
| Molecule Diameter | 7.1 Å |
| Nearest-ncighba distance in Solid $C_{60}$ Crystal | IO.(M A |
| Conductivity | Semiconductor |
| Sublimation Temperature | 300-400 °C |

the stability of these clusters. Fragmentation of all clusters occurs by loss of even cluster fragments, although Young cl al.[31] argued based on collision energy considerations that fragments larger than $C_2$ might have been lost upon impact.

Although photofragmentation and atomic collision studies provided much insight into the Structure of carbon clusters, the dominant fragmentation process in ion engines will likely be duc to impact of $C_{60}$ clusters on discharge chamber walls and electron impact. Studies of $C_{60}$-wall collisions have been conducted by Beck et al.[32], Whetten and Yeretzian[31], Busmann et al.[34,35] and Lill et al.[36]. Theoretical studies of $C_{60}$ surface impacts were performed by Mowrcy et al.[37]. Results of these experiments reported by Beck et al,32 indicate that when $C_{60}$ ions impacted on graphite surfaces no fragmentation was noted even at impact energies as high as 200 cV. Experiments conducted with benzene and naphthalene for comparison using the same experimental apparatus resulted in significant fragmentation even at energies as Jow as 9(J eV[32]. Busmann et al.[34,35] noted fragmentation of $C_{60}^+$ ions only above 130 cV. An attempt to explain the extraordinary stability of $C_{60}$ against fragmentation upon surface impact was made through numerical simulations by Mowrcy et al.[37]. At impact energies up 10 150 CV Mowrcy et al. noted that the spherical $C_{60}$ molecule completely deforms during impact, taking on an extremely oblate shape, however, rebounces back into its original spherical shape after leaving the surface. This observed behavior was termed *resilience* by Beck et al.[32]. Mowrcy et al. further estimated that at 150 CV impact energies roughly 20% of the impact energy is transferred into recoil energy, 25-307. into heating of the cluster and the. remaining energy is dissipated by surface heating. At higher impact energies (200 cV), Mowrcy et al, calculated that nonreactive scattering still accounts for 86% of the surface interactions, with the remainder being sticking and -}1 and -CH pickup. At 250 CV impact energies, fragmentation is observed, only one third of the events arc elastic scattering events and another third of the events is accounted for by sticking to the surface[37].

Resilience of the $C_{60}$ cluster may prove to be a major advantage of this molecule over other heavy ion engine propellants proposed in the past[7,8]. It should be carefully pointed out, however, that no definite conclusions regarding the stability of $C_{60}$ in an actual ion engine can be drawn from these early wall collision experiments yet, First, $C_{60}$ mole.cu]cs will most likely experience multiple wall collisions before being extracted out of the ion engine, as opposed to being subjected 10 single collision events as in those experiments discussed in the previous paragraph[32-37]. Secondly, all previous collision experiments were performed with $C_{60}$ ions[32-37], positive and negative, only and no investigations of neutral $C_{60}$-wall collisions have been performed yet. Third, in Deck's et al.[32] experiment, the $C_{60}$

molecules arc cooled in a helium flow after desorption from a $C_{60}$ film coated steel or tantalum surfaces. No such cooling mechanism would be available in an ion engine, where $C_{60}$ is being produced by sublimation from its solid, crystalline form. Whetten and Yeretzian[33], however, noted that >109'0 fragmentation of detected scatterers was observed for jet-cocded beams at 310 eV impact energy, while for oven-generated, uncooled molecular beams this threshold was lowered to only 260 eV. Finally, Beck et al.[32] pointed out in their investigation that only those collision fragments could be detected with the.ir experimental apparatus that were generated within 2 µs upon impact, thus allowing the possibility for metastable fragmentation after this time period. During their numerical simulations, Mowrey et al.[37] also noted that Calculations were only performed over a time period up to 930 fs, leaving open the possibility for metastable fragmentation in their simulations as well. These findings underline the importance of actual $C_{60}$ ion engine testing in order 10 fully evaluate the feasibility and performance potential of this thruster concept. Initial results obtained during small scale $C_{60}$ engine. tests will be discussed in the next section.

## Current Status of $C_{60}$ Engine Testing:

Currently, $C_{60}$ ion engine tests arc being performed in the United States at the Jet Propulsion Laboratory (JPL) and Busek Co., MA[38,39]. Activities in $C_{60}$ ion engine research have been initiated in Japan[40] and there arc reports of C60 thruster tests being conducted in Russia[27]. However, no details of the work being performed in Japan and Russia arc known yet and this review will therefore focus on US research only. Anderson[41,42] recently initiated experiments with small-scale stainless steel and graphite sources. Anderson's experiments arc described in detail in Ref. *42*. Briefly, 11 mA beam current could be generated with the stainless steel source at 50 V discharge voltage and 0.12 A discharge current. Oscillations in the discharge voltage were observed in intervalls of several minutes, possibly duc to soot formation on discharge chamber wall surfaces[41]. Temperatures of up to 1000 'C were, necessary to provide sufficient fullerene flow rates into the discharge chamber, possibly causing the. fragmentaion of fullerenes observed. Since it was speculated that the stainless steel used in the engine design also might have had a catalytic effect on fullerene fragmentation[41], tests with a graphite source were conducted. Discharge voltages could be lowered to 35 V but showed a similar transit.nt behavior as for the stainless sled source. Due to an improved arrangement of the discharge chamber with respect to the effusive. cell, serving to sublimate the solid fullerenes, only 600 'C were required to provide sufficient flow rates. Figure 2 shows the graphite source. The graphite components themselves arc not visible since they arc surrounded by a stainless steel heat shiled. Recognizable arc three solenoids providing the magnetic field for the engine.

At Busek Co., a $C_{60}$ source manufactured entirely from quartz was tested[38,39]. Interestingly, not only the discharge chamber was made out of quartz but also the C60 vaporizer and, in an earlier version of the experiment, the grids, which were gold plated to make them conductive and later replaced by molybdenum and stainless sled grids. The source, had a diameter of 3.5" and discharge chamber length of 4" and functioned according to the electron bombardment principle, using a cathode (tungsten filament) and an annular stainless steel anode. Using a mix of $C_{60}$ and $C_{70}$ at a ratio of *80% to 20%,* a beam current of 20 mA was drawn from the source at beam ion costs of 915 eV. This value is high even for a small, unoptimized ion engine and is related to the. high discharge voltages required to sustain the fullerene discharge. Discharge voltages around 200 V were required at times to operate. a discharge.. This fact was attributed to cathode poisoning. After operating the tungsten filament cathode in a fullerene discharge, the filament was coated with layers of a graphite soot. This increased the discharge voltage over its 1owcsL measured value of 40 V when the cathode was clean at the beginning of the test. No fragmentation of $C_{60}$ was noted during operation of the engine, except in areas near the. cathode. This conclusion was drawn from deposits found coating various engine parts as well as a cooled collector plate mounted downstream of the engine grids. It is further interesting to note that during these experiments no evidence was found that $C_{60}$ fragmentation is being catalyzed by such materials as stainless steel, molybdenum, boron nitride, alumina or quartz.

As can be seen from these. early thruster tests, $C_{60}$ ion engine technology is still in its infancy. None. of the thruster designs used so far have been optimized for performance and arc usually small scale models used for proof-of-concept typo studies, While performance optimization is certainly a future goal, several feasibility issues still remain 10 be resolved before then. As became clear during these early experiments and was pointed out by Leifer et. al.[8], issues regarding fragmentation of $C_{60}$ under operating conditions typical for an ion engine, condensation of $C_{60}$ at discharge chamber' surfaces and sputtering of engine components by C60 ions remain to be investigated in greater detail.

I

Condensation of $C_{60}$ could pose a problem if conventional electron bombardment (Kaufmann) type thrusters arc being used. Since $C_{60}$ is a semiconductor, condenses on electrode surfaces could impair thruster operation in addition to potential clogging problems of the propellant feed system[8]. in this case, the usage of a radio frequency ion thruster and using heated propellant lines have been suggested[8].

## Propellant Feed Systems for Fullerenes:

During the initial testing Of $C_{60}$ engine concepts as dc.scribed above, the propellant feed system simply consisted of a effusive cell, in which the entire propellant reservoir was heated, causing solid $C_{60}$ to sublimate and enter the, discharge chamber by means of diffusion. While such a relatively simple feed system is appropriate for early proof.of-concept tests attempting to demonstrate the feasibility of a $C_{60}$ ion engine, it is insufficient to demonstrate the feasibility of an entire $C_{60}$ ion propulsion subsystem and definitely not appropriate for actual space missions. }Jc.sting the entire propellant reservoir is wasteful in terms of power expended, lowering the ovc.rail efficiency of the system.

Onc possible solution to this problem is to transport solid $C_{60}$ out of the propellant tank to the. engine by pumping a $C_{60}$ slurry (see Figure 3) out of the propellant tank into the effusive cc]]. $C_{60}$ slurry would be pumped through a filter, comparable to propellant filters in usc today for chemical propulsion systems. $C_{60}$ would remain in the filter which al the same time serves as an effusive cell, providing the engine. with C60 vapor. By adjusting the heating profile. properly, $C_{60}$ vapor will leave the cell through the orifice connecting it with the discharge chamber. As $C_{60}$ is being used up, new fullerenes arc being transported through the slurry to the cell. The liquid transporting the fullerenes could either be rcc ycled or dumped overboard to reduce spacecraft mass.

A second concept would involved compressed fullerenes that arc pushed through a barrel directly into an effusive cell (Figure 4). This feed mechanism would be spring loaded for simplicity and C60 is being moved down the barrel as it vaporizes out of the. cell. Since the C60 is held in place by the barrel, it dots not necessarily need to form a stable rod, In both cases it is crucial to the success of the designs to ensure that $C_{60}$ being vaporized leaves the. diffusive cell only through the orifice connecting it with the discharge chamber and no leakage occurs elsewhere. Experimental testing is obviously necessary to determine the. feasibility of these concepts.

## $C_{60}$ Production:

In order to serve as an electric rocket propellant, sufficient quantities of fullerenes, produced at low cost, would have to be available. Since $C_{60}$ is the most stable and the most abundant of all fullerenes, it is the fullerene of choice for potential propulsion applications. As was pointed out earlier, initial methods of $C_{60}$ production were limited to laser vaporization of graphite targets, able. to produce only microscopic quantities of $C_{60}$ vapor. Krätschmer's experiment[18] allowed the production of macroscopic quantities of solid fullerenes using resistive heating of graphite rods. Quantities of fullerenes produced, however, still remained limited to roughl y 100 mg pcr day. The yield was subsequently increased by other researchers, using modifications to Krätschmer's experiment [18,43,44]. Hauffler et al.[43] was able to increase the $C_{60}$ quantities to several grams pcr day by using an arc discharge between graphite electrodes rather than using resistive heating. The yield of fullerenes in the soot collected amounted to 10 ± 2%.

These yields were increased by Parker et al.[44] to 44%. Modification in this experiment Were related to optimizing the arc discharge. A DC power supply was used and the gap between the electrode optimized to about 4 mm for maximum yield. Typical operating conditions for the arc were 18 V at 60 A ( roughly 1kW power consumption). Two different electrodes were used, onc 1/4" (6.35 mm) in diameter while the second electrode was 1/2" (12.7 mm) in diameter. Only the 1/4" electrode was consumed in the process at a rate of 0.2 in/min (5mm/min). In addition to optimizing the arc discharge, a static He atmosphere at 200 Torr (266.64 kPa) was used rather than a flowing system, which could pump away fullerenes that had not condensed yet. Other modifications to increase the yield of fullerenes included the placement of shims inside the reaction chamber to increase the surface area available for condensation and proper selection of solvents to separate fullerenes and soot.

Despite recent advances made in the development of high yield fullerene production, the delivered quantities arc still completely insufficient for propulsion applications, particularly large scale SEI-type missions. Krätschmer's method and variations thereof[18,43,44] still involve a high fraction of manual labor when scraping the soot from condenser surfaces. This process would therefore have 10 be mechanized and scaled up to yield larger quantities of fullerenes as required by propulsion applications.

Currently, soot containing 12% fullerenes by weight is available for roughly $30 pcr gram[41]. Producing larger quantities of fullerenes should lower costs. An additional opportunity to lower costs would be 10 vaporize coal in an arc discharge rather than graphite since coal is significantly cheaper than graphite[26]. Yields from the vaporization of coal ranged up to 8.6% of fullerenes by mass in the soot collected versus 9.3% from graphite under identical conditions[26]. A completely different way of producing fullerenes was discovered recently by Howard et al.[45] who identified fullerenes in the soot produced by hydrocarbon flames. Yields were as high as 9% of fullerenes pcr soot mass depending on operating conditions and 0.3% pcr fuel carbon mass. This process appears to be easily scalable to produce larger quantities of fullerenes.

A major driver in the production of large scale quantities of fullerenes will also be the potential for application of $C_{60}$ and related fullerenes in areas other than propulsion, such as the recent discoveries of superconductivity in doped $C_{60}$ films[16,28-30]. New technologies like these may significantly increase the demand for fullerenes and contribute to increased fullerene production capabilities. If, however, these production capabilities remain insufficient for the needs of propulsion applications, and in particular large scale SE1-type missions, providing additional production capabilities might significantly contribute to the development cost of large scale $C_{60}$ ion engine technology.

## Summary:

This survey of current activities in $C_{60}$ ion engine testing and the review of several other feasibility issues involved in the development of fullerene thrusters shows that $C_{60}$ ion engines clearly have to be classified as "advanced propulsion systems", i.e. they are not readily available and, in certain areas at least, still require substantial development efforts. When analyzing the performance potential of large scale $C_{60}$ ion engine technology, and when applying results obtained from this study to SEI-type mission scenarios, the early development status of this technology should be recognized. The analytical model to be described in the next chapter will therefore only rc.present an estimate of the performance characteristics of large scale $C_{60}$ ion technology, based on the preliminary experimental data obtainable today.

# ANALYSIS

## Approach:

The analytical model presented in this chapter estimates thruster performances, such as thrust, mass, input power, efficiency and specific mass with specific impulse being the independent variable. The objective of this analysis is to determine these engine parameters for cases in which thrust has been maximized for a given engine, Calculations arc performed for $C_{60}$ propellant as well as the inert gases argon, krypton and xenon, This mode] was based on an earlier analysis made by Leifer et al.[11] which in turn relied in part on Brophy 's model[9]. The ion engine type modeled in this study is of the ring-cusp, electron, bombardment type. However, specific ion production schemes arc not modeled in this analysis and arc simply accounted for by a "lumped" ion production energy input parameter. Data obtained for non-mass related variables arc therefore representative of other ion thruster types as well when adjustments of specific thruster input parameters such as ion production energy or mass utilization arc made. Mass estimates arc based on a model developed by Aston et al.[46,47] for ring-cusp engines. Both two and three grid systems arc mode.tcd.

Several design restrictions were placed on the model. A maximum span-to-gap ratio, i.e. the ratio of grid diameter to grid spacing, of 500 was assumed. This value is consistent with current grid technology[46,47] and accounts for the fact that for a given grid spacing the grid diameter cannot be increased arbitrarily duc to thermal expansion and deflection of the grids. It should be pointed out, however, that future advances in grid technology, such as using carbon-carbon grids, may increase this value, Other restrictions arc placed on the mimimum allowable grid spacing chosen in accord with other studies[11,46,47] to 0.6 mm. The maximum allowable field strength between the grids was assumed as 3000 V/mm in order to avoid grid breakdown[11,46-48]. This electric field strength was held constant throughout the calculations for simplicity. This is an idealizing assumption, since the breakdown field strength actually drops with increasing grid spacing and the results obtained using this model should therefore be interpreted as an approximation. Grid diameters were varied between 50 cm and 100 cm, Fifty centimeter ion engines arc already under development[49]. The upper grid diameter boundary was picked somewhat arbritrarily. Only one case of experimental testing of an ion engine larger than 1 m diameter exists. The 1.5 m dia. NASA Lewis engine was run in the early *1970's* on mercury. However, difficulties were encountered when trying to maintain a stable discharge[50]. By limiting the upper grid diameter boundary to a value less than that of the NASA Lewis engine, a compromise was attempted between conducting a study conservative enough to be credible while still allowing for sufficient flexibility for potential future thruster developments.

The algorithm governing this model is explained in detail below. Briefly, the calculation procedure is divided into two regimes, covering different specific impulse ranges and determined by the design restrictions given above. In both ranges, the objective is to maximize thrust for a certain specific impulse value. In the first range, for a given specific impulse the required beam voltage is calculated and, based on the. breakdown condition for the grids given above, the grid spacing is determined. The net-to-total voltage ratio has been set to its lowest value of R=0.2 in this range to allow for the highest thrust density. For the mentioned maximum allowable span-to-gap ratio the maximum grid diameter is determined. Using grid perveance data, the maximum allowable beam current is calculated, which determines such parameters as thruster input power and thrust.

In the first range the maximum allowable engine size is determined which will yield the maximum thrust for the specified specific impulse. This talc.ulalion procedure is repeated until an engine diameter of 1 m has been reached. At this point, the second regime begins were (he diameter is held constant at 1 m and the net-to-total voltage ratio is being increased from its initial value of 0.2 to its final value of 0.9. Although beam divergence increases with lower net-to-tolal voltage values, it has been assumed in this analysis to be constant throughout the calculations al a value of 95?o[5]1. Since the engine diameter remains fixed at 1 m, thrust is now increased by raising beam voltage and the speci fic impulse value only. Beam current, beam current density, discharge current and propellant consumption arc all assumed to remain constant in this regime.

Within the second regime, at a net-to-total voltage ratio of R=0.55, a switch is made from a three grid system used at lower R values 10a two grid system for higher R values. This change is motivated by results obtained from experiments performed by Rawlin and Hawkins[51,52] using a 30-cm mercury ion thruster. For R values less than *0.55,* a rapid increase in accelerator drain current has been noted for two grid optics. Improved beam optics for a three grid system allows operation to R values as low as 0.2[51,52]. It should be noted, however, that more recently two grid systems have been operated successfully at R values less than 0.55,

In order 10 minimize thruster mass, at an R value of 0.55 and above, the three-grid system is replaced by a lighter weight two-grid system. The upper boundary of 0.9 for the net-to-total voltage ratio is given by the minimum negative voltage that can be applied to the accelerator grid of the two-grid system without causing electron flow into the thruster from the neutralizer discharge[5]]. Therefore, with the exception of the change in grid systems, in the second regime one thruster configuration (1 m diameter) is modeled over a range of operating conditions.

## Governing Equations:

The governing equations in this model have been derived by Blandino[11] during an earlier investigation of high power electric propulsion devices. They arc repeated here. for convenience.

*Regime I:* in the first regime, beam voltage may be expressed in terms of specific impulse using the standard energy balance equation between the electrostatic and kinetic energy of the ions, Taking into account neutral particle losses and thrust divergence losses, yet neglecting multiple charged ions, one obtains

$$V_B = \frac{m_i}{2e}\left(\frac{gI_{sp}}{\eta_u \delta}\right)^2 \qquad (1)$$

which can be written as

$$V_B = C_0 I_{sp}^{\ 2} \qquad (2)$$

with

$$C_0 = \frac{m_i}{2e}\left(\frac{g}{\eta_u \delta}\right)^2 \qquad (3)$$

The twain current is determined by

$$I_B = j A_B \qquad (4)$$

The average current density can be written as

$$j = f_b\,(NPPH)\sqrt{\frac{131.2}{M_W}}\left(\frac{4}{\pi}\right)\frac{V_T^{3/2}}{l_e^2} \qquad (5)$$

Here, $V_T$ is the total voltage, i.e. the voltage between screen and accelerator grid, NPPH is the normalized perveance parameter, which allows the perveance equation, Eqn. (5) to fit experimental data and has been taken here as 2.84 x 10-9 $A/V^{3/2}$ in accordnance with other sources in the literature[47]. The square root allows this equation to be used for other gases than xenon for which is was originally derived. The factor $f_b$ is the beam flatness parameter. It takes into account the fact that the beam current density is not uniformly distributed across the grid diameter, but rather peaks at the grid center. The relationship between maximum and average current density is

$$f_b = \frac{+}{-_{max}} \qquad (6)$$

The variable $l_e$ in Eqn. (5) is defined as the effective acceleration length and follows from the screen-accelerator grid gap $l_g$ and the screen grid hole diameter $d_s$ through a simple geometric relationship as

$$l_e = \sqrt{l_g^2 + \frac{d_s^2}{4}} \qquad (i')$$

For state-of-the-ar( grids it was assumed for the screen grid ho]c diameter[47]

$$d_s = l_g/0.3 \qquad (8)$$

which in the case of a minimum grid gap of 0.6 mm would give minimum screen hole diameters of 2 mm. Current screen grid designs have hole diameters as little as 1.9 mm which agrees reasonably well with the assumption used in Eqn. (8). Inserting Eqn. (8) into Eqn. (7) gives

$$l_e^2 = 3.778\ l_g^2 \qquad (9)$$

Using the maximum allowable electric field strength $E_m$ between screen and accelerator grid, the maximum allowable total voltage between those grids can be determined as

$$V_{T,max} = \frac{E_m}{l_g} \qquad (10)$$

Inserting Eqn. (9) into Eqn. (5), using Eqn. (10) to substitute for $l_g$, assuming a value of $V_{T,max}$ for $V_T$ in Eqn. (5) since we are interested in maximizing the thrust density of the engine and finally using the relationship

$$R = \frac{V_B}{V_T} \qquad (11)$$

for the net-to-total voltage ratio yields

$$j = f_b\frac{(NPPH)}{3.778}\sqrt{\frac{131.2}{M_W}}\left(\frac{4}{\pi}\right) E_m^2\, R^{1/2}\, V_B^{-1/2} \qquad (12.)$$

Substituting for $V_B$ from Eqn. (2) one obtains

$$j = C_1\frac{R^{-1/2}}{I_{sp}} \qquad (13)$$

where the constant $C_1$ is written as

$$C_1 = f_b\frac{(NPPH)}{3.778}\sqrt{\frac{131.2}{M_W}}\left(\frac{4}{\pi}\right)\frac{E_m^2}{C_0^{1/2}} \qquad (14)$$

The final step to obtain an expression for the beam current now consists of evaluating $A_B$. The total grid area can be written as

$$A_g = \frac{\pi}{4}D_g^2 = \frac{\pi}{4}\left[\frac{s}{g}\right]^2 l_g^2 \qquad (15)$$

where [s/g] is the span-to-gap ratio, always taken at its maxiumum value of 500 to maximize thrust. The beam area now relates to the total grid area by incorporating the open area fraction $\Phi_S$ for the screen grid:

$$A_B = \phi_S A_g \qquad (16)$$

Using relations (15), (10), (11) and (2) one can find for the beam area

$$A_B = C_2\frac{I_{sp}^4}{R^2} \qquad (17)$$

where $C_2$ is written as

$$C_2 = \frac{\pi}{4}\left[\frac{s}{g}\right]^2\frac{\phi_S}{E_m^2}C_0^2 \qquad (18)$$

Inserting Eqns (13) and (18) into Eqn. (4) finally gives for the beam current

$$I_B = \frac{C_1 C_2}{R^{3/2}} I_{sp}^3 \qquad (19)$$

Since with Eqn. (13) the maximum available beam current density was calculated, the beam area determined by Eqn. (17) represents the smallest beam area able to produce the beam current determined by Eqn. (19). Given an expression for the beam current, the thruster input power may now be calculated. The thruster input power can be written as

$$P_I = I_B \left[V_B + \varepsilon + V_{NC}\right] + P_{Heat} \qquad (20)$$

Here, ε represents the beam ion production costs expressed in eV/ion or W/A, $V_{NC}$ is the neutralizer coupling voltage and this term in Eqn. (20) accounts for power losses due to beam neutralization. In addition, there are other, small power losses associated with heating of various engine components such as hollow cathodes and neutralizers. Since these power losses are small and occur only temporarily during engine operation, they have been neglected. Note, however, that for C60 engines other power losses occuring during heating of the C60 propellant and propellant feed lines might not be negligible and might have to be included. For the case of $C_{60}$, only the heat required to sublimate the propellant has been taken into account since it was difficult to estimate feed line heaters without knowing the exact engine configuration. The power required for sublimation of $C_{60}$ may be written as

$$P_S = \Delta H_S \frac{\dot{m}}{M_W} \qquad (21)$$

where $\Delta H_S$ is the required heat of sublimation for $C_{60}$ and $\dot{m}$ is the propellant flow rate. $M_W$ in this case is the molar weight of $C_{60}$, i.e. 720 g/mole. For $\Delta H_S$ a value of 43.01 kcal/mole (1 80.1 kJ/mole) was used[53]. This value seems to agree well with other data in recent literature on this subject[54,55]. The total heat requirement for sublimation of $C_{60}$ is then

$$P_{Heat} = \frac{1}{\eta_{Heat}} P_S \qquad (22)$$

where $\eta_{Heat}$ is the efficiency of the effusive cell, taking into account heat losses from the cell. However, since propellant feed mechanisms for fullerene propellants do not yet exist, $\eta_{Heat}$ cannot be accurately determined yet and in the following only $P_S$ has been calculated. As will be shown, the power required to sublimate $C_{60}$ propellant is so small compared to the power required for beam acceleration, that even neglecting the heat loss term in Eqn. (20) has an almost unnoticable effect on the calculation of the thruster input power.

Using Eqn. (2) and (19) in Eqn. (20) yields

$$P_I = C^* C_1 C_0 I_{sp}^5 + C_2 C_1 (\varepsilon + V_{NC}) I_{sp}^3 + P_{Heat} \qquad (23)$$

The remaining performance parameters to be determined are thrust and thruster efficiency. For the thrust we obtain

$$T = \frac{I_B m_i g}{e \eta_u} I_{sp} \qquad (24)$$

taking into account thrust losses due to diffusion of neutrals. Inserting the relationship (19) for $I_B$ gives

$$T = \left(\frac{C_2 C_1 m_i g}{e \eta_u}\right) R^{-3/2} I_{sp}^4 \qquad (25)$$

Thruster efficiency is defined as

$$\eta_T = \eta_{el} \eta_u \delta^2 \qquad (26)$$

which includes electric losses, neutral particle losses and thrust divergence losses. The electric efficiency $\eta_{el}$ can be written as

$$\eta_{el} = \frac{I_B V_B}{I_B (V_B + \varepsilon + V_{NC})} = \frac{1}{1 + \frac{\varepsilon + V_{NC}}{V_B}} \qquad (27)$$

Inserting the expression (2) for $V_B$ finally gives

$$\eta_T = \frac{1}{1 + \frac{\varepsilon + V_{NC}}{C_0} I_{sp}^{-2}} \qquad (28)$$

Remaining thruster performance parameters, such as specific mass and thrust-to-power ratio are easily derived from the expressions given above:

$$\alpha = \frac{M_E}{P_I} \qquad (29)$$

$$[T/P]=\frac{T}{P_t} \tag{30}$$

Finally, discharge currents were calculated for the engine, which follow from an expression derived by Brophy[9]

$$I_D=I_B\left(1+\frac{\varepsilon}{V_B}\right) \tag{31}$$

Using Eqns. *(2),(13), (17), (19), (23), (25), (28)* and (29) through (31), the algorithm as discussed above for Regime I follows easily. All thruster performance parameters have been expressed in terms of the specific impulse as the independent variable. The beam area $A_B$ is also a function of $I_{sp}$ as a result of the design restrictions imposed on this model. Thruster beam area increases with the specific impulse and the model calculates the smallest thruster able to generate the maximum available thrust at this specific impulse 'value (based on the design restrictions given above). As the thruster beam area reaches a value of 1 m diameter, calculations in Regime I arc terminated and calculations arc continued in Regime II.

*Regime 11:* In Regime 11, thruster diameter is assumed constant at 1 m diameter and further thrust increases arc achieved by increasing the net-to-total voltage ratio, R. R is increased by increasing the beam voltage $V_B$ only, while $V_T$, the total accelerating voltage between screen and accelerator grids remains constant at its maximum allowable value for the given grid spacing. This implies that the current density, j remains constant, since j dots not depend on $V_B$. Constant beam area and current density yield constant beam current, discharge current and propellant flow rate. Furthermore, for the specified span-lo-gap ratio, the grid spacing remains unchanged in Regime 11. Thruster mass also remains constant with the exception of the data point at R=0.55 when the three-grid system is being replaced by the two-grid system which causes a mass reduction. Therefore, one, easily derives for Regime II from the expressions given above

$$A_B=const. \tag{32}$$

$$I_B=const. \tag{33}$$

$$I_D=const. \tag{34}$$

$$j=const. \tag{35}$$

$$V_T=const. \tag{36}$$

$$I_g=const. \tag{37}$$

and

$$P_t=I_B\left(C_0\ 1:,4-\ \varepsilon+V_{NC}+P_{Heat}\right. \tag{38}$$

$$T=I_B\left(\frac{m_i g}{e\eta_u}\right)I_{sp} \tag{39}$$

and Eqns (2) and *(28)* through *(30)* remain unchanged.

The algorithm for the model described by Eqns (1) through (39) di ffers somewhat from the model developed by Leifer et al. ][1], In their model, the first regime was used up to the specific impulse value where the discharge current reached a speci fied value, assumed to be 500 A. This approach allowed grid diameters to increase significantly beyond 1 m diameter. Calculations then proceeded in a second regime precisely as discussed here. After that, a third regime was added where the net-to-lotal voltage ratio was held constant and thrust was increased by increasing both beam voltage and total voltage in exactly the same ratio. In order to maintain the constant maximum discharge and beam currents, thruster beam arc had to grow further since current density decreases for constant R but increasing beam voltage (decreasing total voltage) (see Eqn. (13)). This approach final l y led to beam diameters in excess of 2 m. Because of the discussion made above regarding large diameter ion engines, the algorithm in this study was changed according y.

## Input Parameters:

Input parameters to the model for the various propellants arc summarized in Table 2. Neutralizer coupling voltage, ionizer chamber length, open area grid fraction, beam flatness parameter and the divergence thrust loss factor have been kept constant throughout the calculation< and have been assumed to be the same for all propellants as 20 V, 0.20 m, 75%, 0.6 and 0.95, respectively. The open area screen grid fraction is somewhat optimistic; recent grid technology shows screen grid open arc fractions around 67%. Data for propellant utilization efficiency and discharge voltage for the three inert gas propellants were taken from Rawlin[56]. These data arc based on measurements taken with a 30-cm J-series thruster.

Beam ion production cost of 150 eV/ion were assumed for all inert gas propellants, a little lower than most of the data obtained for the 30-cm class thruster[56], taking into account lower expected losses for larger diameter thrusters. For simplicity these values were kept constant, throughout the calculations. Strictly, this assumption is not correct and the calculations performed can therefore only be regarded as an approximation. However, due to the large power consumption by the accelerator system of these large scale thrusters, changes in beam ion production cost, accounting for discharge chamber losses, hardly affect the obtained results.

Estimating values for the propellant utilization and beam ion production costs for $C_{60}$ proved to be more difficult. Leifer et al.[8] recently estimated beam ion production costs of 90 eV/ion for a 30-cm class thruster using Brophy 's model[9]. Using the same approach, however, relying on new data for ionization cross sections by electrons and a numerical calculation for the primary electron utilization factor, Torres et al.[57] estimated beam ion production cost in excess of 180 eV for a 13-cm thruster. The discrepancy between these two data sets may also ly be explained, in part, by the fact that larger thrusters commonly result in lower beam ion production costs due to smaller wall losses per beam ion.

Obviously, none of these estimates compares well with the preliminary experimental data of 900 eV/ion discussed earlier[38-42]. However, the early experimental data obtained so far do not readily lend themselves to extrapolation for performance-optimized, large scale (> 50 cm diameter) engines. None of the small scale thrusters tested was optimized for performance and they only served proof-of-concept type studies. For example, the JPL $C_{60}$ thrusters used grids with only 19, 1/8" holes on both, screen and accelerator grids. This design, although justifiable in terms of simplicity and low cost of small scale engine testing, certainly does not compare favorably with state-of-the-art grid designs. Even for small 15 cm thrusters, open area fractions of 67% are being obtained by placing over 4000 holes on each grid. For these reasons, the estimates obtained with Brophy's model were taken as a guideline and the value obtained by Leifer's et al.[8] study was used, rounded up to a round figure of 100 eV/ion, since it was the one calculated for the larger thruster, Obviously, this is only a very approximate assumption, likely required to be updated new data for this parameter become available. As mentioned earlier, however, for high power ion engine applications, such as the ones discussed in this model, errors introduced by this approximantion are minor since most of the power is used for ion acceleration.

Propellant mass utilizations for large scale $C_{60}$ thrusters are obviously not known either. Estimates obtained by Torres et al .57 for the 13-cm engine indicate propellant utilization efficiencies as high as 0.9 for reasonably low beam ion production costs. The same value was used throughout these calculations for $C_{60}$. As for the inert gas propellants, the input data for propellant utilization and beam ion production costs were held constant throughout the calculations.

## RESULTS

Total power consumption, i.e. thruster input power $P_I$, versus specific impulse for the different propellants $C_{60}$, xenon, krypton and argon is shown in Figure 5. Several important observations can be made by studying this figure. First, although the data cover a thruster diameter range from 50 cm to 100 cm for all propellants, the thrusters deliver substantially different specific impulses for the different propellants. As expected, the heavy $C_{60}$ propellant can only deliver specific impulse values in the range from 1000 to 3000 seconds within the design restrictions included in the model, since the voltages that can be applied *over* the given grid spacings are not sufficient to accelerate the heavy molecule to greater velocities. Accordingly, xenon data range from 2500 to 7500 seconds, krypton values from 3000 to 9500 seconds and argon data from 4000 to 12,000 seconds.

Secondly, total power consumption for the $C_{60}$ thruster is significantly lower than those for the inert gas thrusters. A 1-m $C_{60}$ thruster only requires 80 kW at maximum specific impulse while a xenon thruster of the same size requires up to 200 kW at its maximum specific impulse value. This result is not surprising at all as can be found by inspecting Eqn. (3) and (38) closer. Eqn. (38) describes the thruster input power in Regime II, corresponding to the upper ranges of power levels depicted in Figure 5. As can be seen from Eqns (3) and (38), the input power is a function of the ion mass and the square of the specific impulse, obviously following directly from an identical relationship for the kinetic beam energy.

Table 2: Input Parameters for the Analytical Thruster Performance Model

| | | Propellant |
|---|---|---|

| Input Parameter | $C_{60}$ | Xenon | Krypton | Argon |
|---|---|---|---|---|
| $M_W$ (g/mole) | 720 | 131.30 | 83.80 | 39.948 |
| $m_i$ (kg) | $1.2043 \times 10^{-24}$ | $2.1962 \times 10^{-25}$ | $1.4017 \times 10^{-25}$ | $6.6819 \times 10^{-26}$ |
| $\varepsilon$ (eV/ion) | 100 | 150 | 150 | 150 |
| $\eta_u$ | 0.90 | 0.90 | 0.88 | 0.78 |
| $\delta$ | 0.95 | 0.95 | 0.95 | 0.95 |
| $V_D$ (v) | 35 | 36 | 44 | 46 |
| $V_{NC}$ (V) | 20 | 20 | 20 | 20 |
| $f_b$ | 0.6 | 0.6 | 0.6 | 0.6 |

Thus, increasing the mass of the propellant will have a much lesser impact on the power consumption than increasing the specific impulse. Therefore, although the lighter propellant thrusters can operate at a much larger specific impulse, this increased specific impulse has to be paid for by a significantly increased power requirement. Also visible on Figure 5 is the boundary between Regimes I and II, recognizable by the sharply changing slopes of the. power curves.

In addition to operation at higher specific impulses, the lower thruster efficiencies of the lighter inert gas engines also contribute somewhat to the increased power requirement. Figure *6 shows* the relation ship between thruster efficiency and specific impulse for the various propellants. Notable are the high projected thruster efficiencies for the heavy propellant $C_{60}$ and the correspondingly lower efficiencies for the lighter propellants. The impact of high propellant mass on thruster efficiency has been alluded to in the introduction and can now also be quantitatively explained by inspecting the mathematical relationship obtained for the thruster efficiency in the previous section. Eqn. (28) in conjunction with Eqn. (3) indicates that higher ion masses result in greater efficiencies. The advantage of $C_{60}$ engines in this regard in the specific impulse range from 1000 to 3000 seconds is obvious from Figure 6.

Note, however, that the specific impulse also enters the equation for the thruster efficiency and may offset the impact of the propellant mass. For a given power, according to Figure 5, lighter propellant engines can be operated at higher specific impulses, as noted above. These higher impulse values also increase the thruster efficiency, so that when comparing the thruster effciencies for different propellants at the same power level the differences are not as great than when comparing efficiencies at the same specific impulse value. In particular for the respective maximum obtainable specific impulse values for the 1-m thruster, the differences in thruster efficiency between xenon and $C_{60}$ have almost completely disappeared due to the much higher obtainable maximum specific impulse for xenon than for $C_{60}$.

Although the latter point made concerning the thruster efficiency seems to indicate that a major advantage of $C_{60}$ engines over inert gas thrusters has been lost, this is not so. Thruster efficiency is an important performance parameter for. an electric thruster because it determines how much power has to be provided for the engine. Thruster e. fficiencies for inert gas thrusters, however, can only be raised to levels obtainable with $C_{60}$ thrusters by operating the inert gas engines at high specific impulses. The required power increase to accomplish this mode of operation for the inert gas thrusters, however, completely offsets any gains achieved for the thruster efficiency. It should be mentioned in this context, however, that the selection of the specific impulse is also mission driven and the choice of specific impulses may therefore be limited.

Figure 7 shows the total thruster power consumption plotted versus thrust. As can be seen, for a given power level the C60 engine is able to provide significantly more thrust than the inert gas engines because of operation at lower $I_{sp}$. At a power level of 80 kW and a thruster diameter of 1 m, the thrust level obtainable for $C_{60}$ is 4 N and for xenon it is roughly 2.5 N (see also Tables A.1 and A.2 in the Appendix). Note, however, that over the range of thrust values considered in Fig. 7, in many cases a comparison between thrusters of equal size cannot be made. For the lighter inert gases engine diameters may be significantly Smaller than for C60. This is a result of the algorithm used in this model, which maximizes thrust for an ion engine and therefore always determines the smallest thruster diameter still able to provide a certain thrust level. In this case, for the same power level as for $C_{60}$, the specific impulse of the inert gas thrusters has to be reduced significantly to accomodate this low power level. This reduces the beam voltage, forcing a reduction in the total accelerator voltage $V_T$ in order to keep the net-to-total voltage ratio above its minimum value of 0.2. A lower accelerator voltage, however, allows for a smaller grid gap and, thus, increased current and thrust density of the grid, decreasing its size.

A similar observation can be made when comparing thrust values achievable with the different propellants for the same specific impulse as shown in Figure 8. $C_{60}$ propellant generates more thrust at a given specific impulse than any of the inert gases. For a specific impulse around 3000 seconds, this thrust increase over xenon is almost four-fold which, because of reasons stated above, in the case of this model, however, is partly due to larger thruster diameters.

An interesting observance can be made when inspecting Figure 7 again. It can be noted that for the highest projected thrust values, where, all engines have a 1 -m diameter and are operated at their maximum R-value of 0,9, this thrust value is identical for all propellants. This result may seem surprising at first, however, is easily explained by inspecting the algorithm of this model discussed above. Concentrating the upper range of thrust values shown in Figure 7 to simplify the discussion, the thrust equation (39) is valid. Note, however, that the specific impulse, as well as, the beam current enter the thrust equation. Both, specific impulse values and beam currents, however, are much higher for the inert gas thrusters and thus offset thrust gains made by $C_{60}$ due to its higher molecular mass. As a matter of fact, since beam current and specific impulse are proportional by a factor $(1/\sqrt{m_i})$, the mass dependency cancels out in the thrust equation, resulting in all engines delivering the identical thrust.

Thus, it seems possible for a given thruster size to offset any thrust gains made by $C_{60}$ due to its higher mass by operating it on inert gases at higher beam currents and specific impulse values. While this is a theoretical possibility, several practical design issues may stand in the way of such a decision, First, as has been discussed earlier, selection of the optimum specific impulse is mission dependent, limiting the available choices. Second, the specific impulse increase has to be paid for by significantly increased power requirements. For a thrust level of 4 N, 80 kW are required for a $C_{60}$ engine but almost 200 kW for a xenon engine with this parameter reaching values of 240 kW and almost 350 kW for krypton and argon propellants, respectivel y. Figure 9 plots the thrust-to-power ratio for the various propellants and illustrates probably one of the most important conclusions obtained from this study. As can be seen, the thrust-to-power ratio for $C_{60}$ engines is higher by a factor of almost 2.S over the corresponding values for xenon over the entire range of thrust levels. These reduced power requirements would result in extensive onboard power plant mass reductions for a $C_{60}$ propulsion system, a trend that is supported by increased thruster efficiencies for the heavier $C_{60}$ propellant discussed earlier, On the other hand, however, it also has to be noted that due to the lower specific impulse capability of $C_{60}$ thrusters propellant mass requirements will increase for a given $\Delta v$. Future mission design studies will have to investigate this trade-off further.

Secondly, as illustrated in Figure 10, the. higher beam currents required for inert gas engines to achieve the same thrust levels as for $C_{60}$ result in large discharge currents for a Kaufmann-type thruster configuration. While even a 1-m diameter $C_{60}$ thruster, operating at a thrust level of 4 N, only requires a relatively benign 50 A discharge current, these values increase to 180 A, 190 A and 260 A for xenon, krypton and argon, respectivel y. It should be carefully noted, however, that discharge current calculations are influenced by the beam ion production costs and that there still exists some uncertainly regarding this parameter for $C_{60}$.

Finally, Figures 11 and 12 show specific mass data which are of particular intersest for mission planners. In Figure 11, specific masses are plotted versus thruster input power. As can be observed, specific mass values for $C_{60}$ thrusters are. higher for lower power levels, since in these cases larger $C_{60}$ engines are compared with smaller inert gas thrusters as discussed above. For higher power levels, as inert gas engines reach the 1-m thruster diameter limit as well, all specific masses converge upon the same value.s for all propellants.

In Figure 12, the same specific mass data are plotted against specific impulses. Here, the $C_{60}$ data stay lower than the. inert gas data, a trend that is followed by the heavier inert gases when compared with the lighter gases. The explanation for this behavior can be found by inspecting Figure 5 again. For the same specific impulse higher power levels are required for the heavier propellants since more energy has to be expended accelerating the heavier ions. As a result the specific mass, i.e. the thruster mass divided by this power level, drops.

Other results obtained in the course of this study were data on thruster masses, ranging between 19 kg and 45 kg, propellant mass flow rates, ranging between 0.043 to 0.12 g/s, 0.019100.052 g/s, 0.016 100.043 g/s and 0.012 to 0.033 g/s for $C_{60}$, xenon, krypton and argon, respectively, demonstrating the well known trend of lower propellant consumption of higher $I_{sp}$ rocket engines. Beam currents for the different propellnat t ypes ranged between 5.16 to 14.64 A, 12.44 to 34.32 A, 15.83 to 42.9 A and 22.79 to 62. 18A for $C_{60}$, xenon, krypton and argon, respectively and emphasize the technological difficulties associated with high thrust inert gas engines. These and other data are summarized in Tables A, 1 through A.4 in the Appendix.

It should be carefully pointed out in the discussion of these results, however, that they are influenced by the initial assumptions made in this model with respect to the maximum span-to-gap ratio, the constant breakdown electric field strength between the grids or beam ion production energies and propellant utilization efficiencies, for example. Changes introduced to these assumptions, whether motivated by improved grid technology, updated $C_{60}$ engine data or replacing some of the simplifying assumptions in the analysis, may all impact the obtained results.

## ` ` , SIONS

The purpose of this study was to investigate. performance characteristics of large scale $C_{60}$ ion engines for potential use on SE1-type missions when compared with similar sized inert gas thrusters. Such an attempt may appear premature regarding the identified early development status of $C_{60}$ ion engine technology. However, considering the important role propulsion will play in SIH-type mission scenarios, dramatically impacting flight time, spacecraft mass and mission cost, an early investigation of this new electric thruster concept appeared justified, in particular when taking into account lime required for development of this engine type. Nonetheless, feasibility issues have to be taken into account when interpreting results obtained from this study. Although previous research has indicated that C60 is a very stable molecule during collisions, fragmentation studies under conditions resembling actual ion engine discharge chamber conditions remain to be conducted in greater detail. Another issue.s of Concern in the development of $C_{60}$ ion engine. technology is possible propellant condensation on engine parts and sputtering of engine components by $C_{60}$ ions also remains to be investigated.

Propellant feed mechanisms fOr $C_{60}$ propellant also require closer attention. Heating the entire propellant reservoir as is the case during current engine testing is not practical for long duration ground testing or actual space flight conditions. Two propellant feed concepts have been suggested, although experimental testing will be necessary to examine their feasibility. Finally, the issue of propellant production may be of some future concern if large quantities of propellnat were needed. As current experience with xenon availability anrt cost have shown[58], propellant availabilty may not be a trivial problem, in particular for Sill-type missions requiring large amounts of propellant.

After a review of these feasibility issue.s and state-of-the-art of $C_{60}$ engine testing, thruster performance parameters such as thrust, power requirement, thruster efficiency, specific mass, thrust-to-power ratio as well as some technologically interesting parameters such as discharge, current, have been calculated using an analytical model with specific impulse being the independent variable. Previously made comparisons of $C_{60}$ engines with inert gas thrusters for near-earth missions have indicated certain advantages of C60 thrusters over their inert gas counter parts, such as higher thrust and thruster efficiency for a given specific impulse or power level. Although these findings remain unchallenged in this study, potential advantages of $C_{60}$ ion technology over inert gas engines for SEI-type mission applications are. more subtle.

While for near-earth applications a specific impulse range between 1 000 and 2000 seconds is preferred in order to keep electric power requirements low while still allowing for substantial propellant mass savings, high Av SIiI-type missions favor higher specific impulse ranges. Therefore, inert gas thrusters may offset some of these efficiency and thrust advantages for $C_{60}$ engines when operated in a higher specific impulse range. $C_{60}$ thrusters could achieve specific impulses higher than 3000 seconds only under great difficulties. High beam voltages would be required to accelerated the $C_{60}$ ion to such high velocities. Since the beam voltage cannot be raised independently from the total accelerating voltage $V_T$ without causing electron impingement on the. accelerator grid from the neutralizer discharge, $V_T$ would also have to be raised, resulting in an increased grid gap. Since a larger grid spacing reduces current and thrust density, it would have to be compensated for by larger grid diameters which ultimately would result in large grid diameters for high $Is_p$ $C_{60}$ engines producing comparable thrust levels.

However, high specific impulse values as well as large beam currents required for inert gas thrusters to achieve thrust values as high as With $C_{60}$ propellant also results in significant problems for inert gas engines. High specific impulse.s will result in large power requirements and large beam currents will require high discharge currents. The high power requirements increase overal 1 spacecraft mass of a space vehicle propelled by inert gas thrusters.

Although the high thrust-to-power ratio of $C_{60}$ engines, being roughly 2.5 times the corresponding value for a xenon thruster of comparable size, leads to much more benign cathode current conditions and significantly reduced power require.rncn[s, the. lower available specific impulses for $C_{60}$ engines also necessitate larger propellant masses for a given Av pcr mission. For the same, thrust, the required mass flow rate of a $C_{60}$ thruster is about 2.5 time.s the mass flow rate for a xenon thruster, while power is reduced by the mentioned factor of 2.5 also. However, since $C_{60}$ may be stored in solid form, an ingeniously designed $C_{60}$ propellant feed system may lead to mass savings over an inert gas propulsion system, due to heavy high pressure tankage required for inert gas propellants. It should be noted, however, that further study is necessary to verify this statement.

The results obtained with this model arc all clearly tied to the initial assumptions made regarding maximum span-to-gap ratio, constant breakdown electric field strength between the grids, or uncertainties regarding ion beam production energies and propellant mass utilization for $C_{60}$ engines. It should therefore be noted that this analysis should only be considered as an approximation based on the.sc assumptions and that changes in ion engine technology, such as grid design, improved data sets on $C_{60}$ engine operation or a more detailed analysis, replacing some of the simplifications rnadc in this mode.1, may affect the obtained results accordingly.

It is recommended that research on this subject continues in the following manner::

1. A mission design study should be initiated, using the data obtained in this study to estimate overall spacecraft masses, power system masses and propellant masses as well as trip limes for $C_{60}$ and inert gas propellants.

2. Experimental testing of $C_{60}$ engine technology should continue. Feasibility issues of fragmentation, propellant condensation and sputtering remain to be studied in greater detail before it can be dctcrmincd if $C_{60}$ ion engine technology is an alternative to inert gas engines. After that, $C_{60}$ engines should bc performance optim ized. Results obtained from these tests will have a very important near term impact on US space technology, as they may lead to the development of smaller scale thrusters for near-earth applications.

3. Parallel 10 the testing of $C_{60}$ ion engines described in Item 3, work should begin on the development on $C_{60}$ propellant feed systems. Improvements over the current approach of heating the entire propellant reservoir arc necessary both for long duration ground testing as well as actual space applications. As with the actual ion engine testing itself, test results obtained from these investigations may benefit near term applications of $C_{60}$ ion engine technolog y.

4. Finally, as a last step in investigating the applicability of $C_{60}$ ion engines for large scale electric space missions, the issue of $C_{60}$ production should be revisited and availability and cost of fullerene propellants have to be reassessed.

None of these items should be viewed indcpcndcnt from the other. Obviously, results from an analysis of required propellant masses for large scale lunar and interplanetary missions have to be viewed critically in terms of propellant availability. Most importantly, *experimental* testing of engine and feed system technology should bc emphasized since only experimental investigations will be able to resolve feasibility issues and provide the data necessary for a further, meaningful study of this concept.

## ACKNOWLEDGEMENTS

The work described in this paper was performed by the J ct Propulsion Laboratory, California Institute of Technology, under contract with the National Aeronautics and Space Administration.

The author would like to thank Stephanie D. I.eifer and John J. Blandino for their help and support in conducting this work.

## REFERENCES

1. Frisbee, R.}]., Blandino, J.J. and Leifer, S. D., "A Comparison of Chemical Propulsion, Nuclear Thermal Propulsion, and Multimegawatt Electric Propulsion for Mars Missions", AIAA Paper 91-2332, 27th Joint propulsion Conference, Sacramento, CA, J uric. 24-26, J 991.

2. Frisbee, R.H., "SP-1OO Nuclear Electric Propulsion for Mars Cargo Missions", JPL Internal Document, JPL D-9676, Pasadena, CA, March 13, 1992.

3. Braun, R. D. and Blersch, D. J., "Propulsive Options for a Manned Mars Transportation

System", *J. Spacecraft*, Vol. *28, No.* 1, Jan.-Feb. 1991, pp. 85-92.

4. Gilland, J.}]., "Mission and System Oplin~i~.alien of Nuclear Electric Propulsion Vehicles for lunar and Mars Missions", IEPC Paper 91-038, 2nd International Electric propulsion Conference, Viarregio, Italy, October 14-17, 1991.

5. Jahn, R, G., "Physics of Electric Propulsion", McGraw-}lill, New York, 1968.

6. Stuhlinger, E., "Ion Propulsion for Space Flight", McGraw-Hill, New York, 1961.

7. Dugan, J. V., "Sonic Theoretical Bases for Selection of Molecular Ion Propellants and a Survey of Molecular Plasma Collision Processes", NASA Technical Note, NASA TN-D-1 185, National Aeronautics and Space Administration, Washington, D. C., February 1964.

8. Leifer, S.D., Rapp, D. and Saunders, W. A., "Electrostatic propulsion using $C_{60}$ Molecules", Technical Note, *Journal of i'repulsion and Power*, Vol. 8, No. 6, Nov.-Dec. 1992, pp.1297-1300.

9. Brophy, J.R., "Ion Thruster Performance Model", NASA CR-17481O, National Aeronautics and Space Administration, Washington, D. C., December 1984.

10. Frisbee, R.H., "Innovative Electric Propulsion Thruster Technologies", JPL-Internal Document, to be published.

11. Leifer, S. D., Blandino, J.J. and Sercel, J. C., "Electric Thruster Models for Multimegawatt Nuclear Electric Propulsion Mission Design", Proceedings of the 8th Symposium on Space Nuclear Power Systems, Albuquerque, NM, January 1991, pp. 482-492..

12. Tucci, 1.., "NASA Shuts Down Human Exploration Shop", Article in Space News, Vol. 4, No. 14, March 29- April 4, 1993, p. 3.

13. NASA Magazine, Summer 1993, p.7.

14. Kiermann, V., "Space Reactor Work Fades for Want of Mission", Article in *Space News*, Vol. 4, No. 16, April 19-25, 1993.

15. Rohlfing, E.A., Cox, D.M. and Kaldor, A., "production and Characterization of Supersonic Carbon Cluster Beams", *J. Chem. Phys.*, Vol. 81, No. 7, October 1984, pp.3322-3330.

16. Huffmann, DR., "Solid $C_{60}$", *Physics Today*, November 1991, pp.22-29.

17. Kroto, H. W., Allaf, A.W. and Balm, S. P., "$C_{60}$: Buckminsterfullerene", *Chem. Rev.*, Vol. 91, No. 6, 1991, pp.1213-1235.

18. Krätschmer, W.;, l.sub, L. D. and Festiropolous, K., "Solid C60: A New Form of Carbon", *Nature*, Vol.347, September 27, 1990, pp.354-357.

19. Kroto, H. W., Heath, J.R., O'Brien, S. C., Curl, R.F. and Smalley, R.E., "$C_{60}$: Buckminsterfullerene", Letters to Nature, *Nature*, Vol. 318, November 14, 1985, pp.162-163.

20. O'Brien, S. C., Heath, J. R., Curl, R.F. and Smalley, R. Ii.,' "Photophysics of Buckminsterfullerene and other Carbon Cluster Ions", *J. Chem. Phys.*, Vol. 88, No. 1, 1988, pp.220-230.

21. Curl, R.F. and Smalley, R.E., "Probing $C_{60}$", *Science*, Vol. 243, November 12, 1988, pp.1017-1022.

22. Weiss, F.P., Elkind, J.I.., O'Brien, S. C., Curl, R.F. and Smalley, R.E., "Photophysics of Metal Complexes of Spheroidal Carbon Shells", *J. Am. Chem. Soc.*, Vet. 110, 1988, pp. 4464-4465.

23. Ben-Amotz, D., Cooks, R. G., Dejarme, 1.., Gunderson, J. C., Hoke, S.H., Kahr, B., Payne, G.L. and Wood, J.M., "Occurance and Fragmentation of High-Mass Fullerenes", *Chemical Physics Letters*, Volume. 183, No.1,2, August 23, 1991, pp.149-152.

24. Kroto, }1., "Space, Stars, $C_{60}$, and Soot ", *Science*, Vol. 244, Novemebr 25, 1988, pp.] 139-1145.

25. Wiedemann, H.G. and Bayer, G., "Thermoanalytical investigations of Fullerenes", *Thermochemica Acts*, Vol. 214, 1993, pp. 85-91.

26. Pang, 1.. S. K., "Fullernes from Coal", Scienti fic Correspondence, *Nature*, Vol.352, August 8, 1991, p. 480.

?.7. 1 .cifcr, S.D., Personal Communication, JPL, Pasadena, CA, August *1993.*

28. Curl, R.F. and Smalley, R.E., "Fullerenes", *Scientific American,* October 1991, pp.54-63.

29. Hebard, A.F., Roseinsky, M.J., Haddan, R.C., Murphy, D. W., Glarum, S.H., Palstra, T.T.M., Ramirez, A, P. and Kortan, A. R., "Superconductivity at 18 K in Potassium-Doped $C_{60}$", Letters to Nature, *Nature,* Vol. *350,* April 18, 1991, pp. 600-601.

30. "Ammonia Intercalation Raises '$J_c$ of Fulleride Superconductor", Article in *C&EN,* April 5, 1993, p.26.

31. Young, A.B., Cousins, L.M. and Harrison, A.G., "A Collisional Study of some $C_{60}$ and $C_{70}$ Fullerne Ions", *Rapid Communications in Mass Spectrometry*", Vol. 5, 1991, pp. 226-229.

32. Reck, R. D., St. John, P., Alvarez, M. M., Diederich, F. and Whetten, R.L., "Resilience of All-Carbon Molecules C60, C70 and C84; A Surface-Scattering Time-of-Flight Investigation", *J.Phys.Chem.*, Vol.95, No.21, 1991, pp. 8402-8409.

*33.* Whetten, R.L. and Yeretzian, C., "Fullerenes under Extreme Temperatures and Stress: Collisions of Fullerenes with Surfaces and with other Fullerenes", *international Journal of Modern Physics B, VO1.6, Nos.23 & 24, 1992, pp. 3801-3814.*

34. Busmann, H.G., Lill, T., Reif, B. and Hertel, I, V., "Collision Induced Fragmentation and Resilience of Scattered $C_{60}^+$ Fullernes", *Surface Science,* Vol. 272, 1992, pp. 146-153.

*35.* Busmann, H.G., Lill, T., Rcif, Il., Hertel, I.V. and Maguire, H. G., " Energy Partition in Collisions of $C_{60}^+$ Ions with Diamond (1 11) and Graphite (0001) Surfaces", *J.Chem. Phys.*, Vol. 98, No. 9, May 1, 1993, pp. 7574-7579.

36. Lill, T., Busmann, H.G., Reif, B. and Hertel, I. V., "Dynamics of $C_{60}^+$ Surface Impact: Rolling, Deformation, Disintegration, and Deposition on HOPG Graphite", *Appl. Phys. A, Vol.* 55, 1992, pp. 461-467.

37. Mowrcy, R. C., Brenner, D.W., Dunlap, B.I., Mintmire, J.W. and While, C.'l"., "Simulations of $C_{60}$ Collisions with a Hydrogen-Terminated Diamond (111} Surface", *J.Phys.Chem.*, Vol. 95, 1991, pp. 7138-7142.

38. Hruby, V., Personal Communication, Buseck Co., Needham, MA, August 1993.

39. Hruby, V., "A Fullerene Hall Thruster Development", Final Report, Phase I - Small Business Innovative Research, Contract No. NAS3-26712, Buseck Co. Inc., Needham, MA, April 1993.

40. Takehara, 11. and Nakayama, Y., "C6 o Molecule as a Propellant for Electric Propulsion", IEPC Paper 93-032, to be presented at the 23rd international Electric Propulsion Conference, Seattle, WA, September 13-17, 1993.

41. Anderson, J., Personal Communication, JPL, Pasadena, CA, September 1993.

42. Anderson, J. and Fitzgerald, D., "Experimental Investigation of Fullerene Propellant for Ion Propulsion", IEPC Paper 93-033, 10 be presented at the 23rd International Electric Propulsion Conference, Seattle, WA, September 13-17, 1993.

43. Hauffler, R.E., Conceico, J., Chibante, L. P. F., Chai, N. E., Byrne, N.E., Flanagan, S., Haley, M. M., O'Brien, S, C., Pan, C., Xiao, Z., Billups, W.E., Ciufolini, A., Hauge, R.H., Margrave, J. L., Wilson, L. J., Curl, R.F. and Smalley, R.E., "Efficient Production of $C_{60}$ (Buckminsterfullerene), $C_{60}H_{36}$, and the Solvated Buckide Ion", *J. Phys. Chem.*, Vol. 94, 1990, pp. 8634-8636.

44. Parker, D.H., Wurz, P., Chatterjee, K., Lykke, K. R., Hunt, J.E., Pellin, M. J., Hemminger, J. C., Gruen, D.M. and Stock, I.. M., "High-Yield Synthesis, Separation, and Mass-Spectrometric Characterization of Fullernes $C_{60}$ to $C_{266}$, *J. Am. Chem. Soc.*, Vol. 11 3, pp. 7499-7503.

45. Howard, J. B., McKinnon, T., Makarovsky, Y., Lafleur, A. I., and Johnson, M. E., "Fullerenes $C_{60}$ and $C_{70}$ in Flames", Letters to Nature, *Nature,* Vol. 352, July 11, 1991, pp. 139-141.

46. Aston, M.B., Aston, G. and Brophy, J.R., "User Interactive Electric propulsion Software Design", AIAA Paper 89-2376, 25th Joint Propulsion Conference, Monterey, CA, July 10-12, 1989.

47. Brophy, J. R., Aston, M.B., and Aston, G., "Detailed Electric Propulsion System Model and Software Development", Contract No. NAS3-25464, Electric Propulsion Laboratory, Inc., Lancaster, CA, December 1989.

48. Kaufman, H.R., "Advances in Electronics and Electron Physics", Vol. 36, Academic Press, 1974, p.309.

49. Rawlin, V.K. and Minis, M.G., "ion Optics for High Power 50-cm-dia. Ion Thrusters", AIAA Paper 89-27)7, 25th Joint propulsion Conference, Monterey, CA, July 10-12, 1989.

50. Nakanishi, S. and Pawlik, E. V., "Experimental Investigation of a 1,5 m-diam. Kaufman Thruster", *J. Spacecraft/,* Vol.5, *No. 7,* July 1968, pp.801-807.

51. Rawlin, V.K. and Hawkins, C.E., "Increased Capabilities of the 30-cm Diameter Hg Ion Thruster", NASA 'I'M-79142, National Aeronautics and Space Administration, Washington, D.C., May 1979.

52. Rawlin, V.C. and Patterson, M. J., "High Power Ion Thruster Performance", Fourth Symposium on Space Nuclear Power Systems, Albuquerque, NM, January 12-16, 1987,

53. Leifer, S.D., Personal Communication, JPL, Pasadena, CA, Summer 1992.

54. Abrefah, J., Balooch, M., Sickhaus, W.J. and Olander, D. R., "Vapor Pressure of Buckminsterfullerene", unpublished draft.

55. Pan, C., Chandradekharasiah, M. S., Agan, D., Hauge, R.H. and Margrave, J.L., "Determination of Vapor Pressure of $C_{60}$ and C70 Mixture", unpublished draft.

56. Rawlin, V. K., "Operation of the J-Series Thruster Using Inert Gas", NASA TM-82977, National Aeronautics and Space Administration, Washington, D. C., 1982. Published as AIAA Paper 82-1929, 16th International Electric Propulsion Conference, New Orleans, Louisiana, November 17-19, 1982.

57. Torres, E.R., Matossian, J. N., Williams, J.D. and Martinez-Sanchez, M., "Prediction of the Performance of an Ion Thruster Using Buckminsterfullerene as the Propellant", AIAA Paper 93-2494, 29th Joint Propulsion Conference, Monterey, CA, June 28-30, 1993,

58. Welle, R.P., "Xenon and Krypton Availability for Electric Propulsion: An Updated Assessment", AIAA Paper 93-2401, 29th Joint propulsion Conference, Monterey, CA, June 28-30, 1993.

## APPENDIX

Table A.1 through A.4 listed below summarize the data obtained for $C_{60}$, xenon, krypton and argon propellant, respectivel y.

Table A. 1: C60 Performance Data

C60.Dat

Tue, Sep 7, 1993 12:05 AM

| | Isp {see) | R | Power (kW) | ?s (w) | T (N) | ETA | MASS (kg) | Alpha (kg/kW) | T / P (N/kW) |
|---|---|---|---|---|---|---|---|---|---|
| 1 | 1'00.000 | 0.200 | 3.710 | 10.780 | 0.470 | 67.660 | 18.430 | 4.950 | 0.125 |
| 2 | 1250.000 | 0.200 | 6.770 | 15.820 | 0.780 | 70.310 | 24.920 | 3.670 | 0.110 |
| 3 | 1300.000 | 0.200 | 8.170 | 17.800 | 0.910 | 71.030 | 27.450 | 3.360 | 0.110 |
| 4 | ?350.000 | 0.200 | 9.770 | 19.930 | 1.060 | 71.680 | 30.180 | 3.090 | 0.108 |
| 5 | 1400.000 | 0.200 | 11.620 | 22.230 | 1.220 | 72.280 | 33.130 | 2.850 | 0.105 |
| 6 | 7450.000 | 0.200 | 13.750 | 24,690 | 1.410 | 72.830 | 36.300 | 2.640 | 0.102 |
| 7 | 1500.000 | 0.200 | 16.180 | 30.580 | 1.610 | 73.300 | 39.700 | 2.450 | 0.100 |
| 8 | 1557.000 | 0.200 | 19.350 | 30.570 | 1.87o | 73.840 | 43.900 | 2.270 | 0.097 |
| 9 | 1600.000 | 0.210 | 20.330 | 30.570 | 1.920 | 74.190 | 43.900 | 2.160 | 0.094 |
| 10 | 1800.000 | 0.270 | 25.230 | 30.570 | 2.160 | 75.570 | 43.900 | 1.740 | 0.085 |
| 11 | 1900.000 | 0.300 | 27.940 | 30.570 | 2.280 | 76.110 | 43.900 | 1.570 | 0.081 |
| 12 | 2000.000 | 0.330 | 30.760 | 30.570 | 2.400 | 76.580 | 43.900 | 1.430 | 0.078 |
| 13 | 2200.000 | 0.400 | 36.840 | 30.570 | 2.640 | 77.350 | 43.900 | 1.190 | 0.072 |
| 14 | 2400.000 | 0.480 | 43.510 | 30.570 | 2.880 | 77.940 | 43.900 | 1.000 | 0.066 |
| 15 | 2585.000 | 0.550 | 50.190 | 30.570 | 3.100 | 78.380 | 43.900 | 0.870 | 0.061 |
| 16 | 2800.000 | 0.650 | 58.550 | 30.570 | 3.360 | 78.790 | 38.750 | 0.660 | 0.057 |
| 17 | 3000.000 | 0.740 | 66.950 | 30.570 | 3.600 | 79.090 | 38.750 | 0.580 | 0.054 |
| 18 | 3200.000 | 0.840 | 75.940 | 30.570 | 3.840 | 79.350 | 38.750 | 0.510 | 0.051 |
| 19 | 3300.000 | 0.900 | 80.650 | 30.570 | 3.960 | 79.450 | 38.750 | 0.480 | 0.049 |

| | TS (K) | mdot (g/s) | ID (A) | IB (A) | lg (mm) | DG (cm) | VB (V) | VT (V) |
|---|---|---|---|---|---|---|---|---|
| 1 | 456.000 | 0.043 | 19.920 | 5.160 | 1.000 | 50.000 | 599.000 | 2994.000 |
| 2 | 453.000 | 0.063 | 29.230 | 7.580 | 1.300 | 64.400 | 773.000 | 3866.000 |
| 3 | 452.000 | 0.071 | 32.880 | 8.520 | 1.400 | 69.700 | 836.000 | 4181.000 |
| 4 | 451.000 | 0.080 | 36.820 | 9.550 | 1.500 | 75.170 | 902.000 | 4510.000 |
| 5 | 449.000 | 0.089 | 41.060 | 0.650 | 1.600 | 80.800 | 969.850 | 4849.000 |
| 6 | 448.000 | 0.099 | 45.620 | 1.830 | 1.700 | 86.700 | 1040.000 | 5202.000 |
| 7 | 447.000 | 0.109 | 50.510 | 3.090 | 1.900 | 92.800 | 1113.000 | 5567.000 |
| 8 | 445.000 | 0.120 | 56.480 | 4.640 | 2.000 | 100.000 | ?200.000 | 5998.000 |
| 9 | 442.000 | 0.120 | 56.480 | 4.640 | 2.000 | 100.000 | 1267.000 | 6000.000 |
| 10 | 442.000 | 0.120 | 56.480 | 4.640 | 2.000 | 100.000 | 1603.000 | 6000.000 |
| 11 | 442.090 | 0.120 | 56.480 | 4.640 | 2.000 | 100.000 | 1786.000 | 6000.000 |
| 12 | 442.000 | 0.120 | 56.480 | 4.640 | 2.000 | 1 00.000 | 1979.000 | 6000.000 |
| 13 | 442.900 | 0.120 | 56.480 | 4.640 | 2.000 | 100.000 | 2395.000 | 6000.000 |
| 14 | 442.000 | 0.120 | 56.480 | 4.640 | 2.000 | 100.000 | 2850.000 | 6000.000 |
| 15 | 442.000 | 0.120 | 56.480 | 4.640 | 2.000 | 100.000 | 3307.000 | 6000.000 |
| 16 | 442.000 | 0.120 | 56.480 | 4.640 | 2.000 | 100.000 | 3879.000 | 6000.000 |
| 17 | 442.000 | 0.120 | 56.480 | 4.640 | 2.000 | 100.000 | 4453.000 | 6000.000 |
| 18 | 442.000 | 0.120 | 56.480 | 4.640 | 2.000 | 100.000 | 5067.000 | 6000.000 |
| 19 | 442.000 | 0.120 | 56.480 | 4.640 | 2.000 | 100.000 | 5389.000 | 6000.000 |

Table A.2: Xenon Performance Data

Xenon.Dat

Tue, Sep 7, 1993 12:00 AM

| | Isp (See) | R | Power (kW) | PS (kW) | T (N) | ETA | MASS (kg) | Alpha (kg/kW) | T / P (N/kW) |
|---|---|---|---|---|---|---|---|---|---|
| 1 | 2600.000 | 0.200 | 9.700 | 0.000 | 0.480 | 63.520 | 18.830 | 1.940 | 0.050 |
| 2 | 2800.000 | 0.200 | 13.630 | 0.000 | 0.650 | 65.490 | 22.390 | 1.640 | 0.048 |
| 3 | 3000.000 | 0.200 | 18.760 | 0.000 | 0.860 | 67.170 | 26.480 | 1.410 | 0.046 |
| 4 | 3200.000 | 0.200 | 25.360 | 0.000 | 1.110 | 68.600 | 31.130 | 1.230 | 0.044 |
| 5 | 3400.000 | 0.200 | 33.730 | 0.000 | 1.410 | 69.840 | 36.430 | 1.080 | 0.042 |
| 6 | 3647.000 | 0.200 | 47.020 | 0.000 | 1.870 | 71.150 | 43.930 | 0.930 | 0.040 |
| 7 | 3800.000 | 0.217 | 50.550 | 0.000 | 1.950 | 71.850 | ,43.910 | 0.870 | 0.038 |
| 8 | 4200.000 | 0.265 | 60.460 | 0.000 | 2.150 | 73.390 | 43.9.10 | 0.730 | 0.036 |
| 9 | 4600.000 | 0.318 | 71.370 | 0.000 | 2.360 | 74.580 | 43.910 | 0.620 | 0.033 |
| 10 | 5000.000 | 0.376 | 83.260 | 0.000 | 2.560 | 75.000 | 43.910 | 0.530 | 0.031 |
| 11 | 5400.000 | 0.439 | 96.140 | 0.000 | 2.770 | 76.290 | 43.910 | 0.460 | 0.029 |
| 12 | 5800.000 | 0.506 | 110.010 | 0.000 | 2.970 | 76.920 | 43.910 | 0.400 | 0.027 |
| 13 | 6050.000 | 0.550 | 119.190 | 0.000 | 3.100 | 77.250 | 38.750 | 0.320 | 0.026 |
| 14 | 6200.000 | 0.578 | 124.880 | 0.000 | 3.180 | 77.430 | 38.750 | 0.310 | 0.025 |
| 15 | 6600.000 | 0.655 | 140.740 | 0.000 | 3.380 | 77.860 | 38.750 | 0.280 | 0.024 |
| 16 | 7200.000 | 0.780 | 166.380 | 0.000 | 3.690 | 78.370 | 38.750 | 0.230 | 0.022 |
| 4₇ | 7600.000 | 0.870 | 184.710 | 0.000 | 3.900 | 78.660 | 38.750 | 0.210 | 0.021 |
| 18 | 7740.000 | 0.900 | 191.360 | 0.000 | 3.970 | 78.740 | 38.750 | 0.200 | 0.02' |

| | TS (K) | mdot (g/s) | ID (A) | IB (A) | lg (mm) | Dg (cm) | VB (v) | VT (V) |
|---|---|---|---|---|---|---|---|---|
| 1 | 624.000 | 0.019 | 64.250 | 12.440 | 1.020 | 50.850 | 610.000 | 3050.000 |
| 2 | 622.000 | 0.024 | 80.240 | 15.530 | 1.170 | 58.970 | 707.000 | 3537.000 |
| 3 | 619.000 | 0.029 | 98.700 | 19.100 | 1.350 | 67.690 | 812.130 | 4060.000 |
| 4 | 6:7.000 | 0.035 | 119.780 | 23.180 | 1.540 | 77.020 | 924.020 | 5216.000 |
| 5 | 613.000 | 0.042 | 143.670 | 27.810 | 1.730 | 86.950 | 1043.100 | 6001.000 |
| 6 | 609.000 | 0.052 | 177.320 | 34.320 | 2.000 | 100.000 | 1 200.000 | 6000.000 |
| 7 | 605.000 | 0.052 | 177.320 | 34.320 | 2.000 | 100.000 | 1303.000 | 6000.000 |
| 8 | 605.000 | 0.052 | 177.320 | 34.320 | 2.000 | 100.000 | 1519.800 | 6000.000 |
| 9 | 605.000 | 0.052 | 177.320 | 34.320 | 2.000 | 100.000 | 1909.400 | 6000.000 |
| 10 | 605.000 | 0.052 | 177.320 | 34.320 | 2.000 | 100.000 | 2255.900 | 6000.000 |
| 11 | 605.000 | 0.052 | 177.320 | 34.320 | 2.000 | "100.000 | 2631.300 | 6000.000 |
| 4₂ | 605.000 | 0.052 | 177.320 | 34.320 | 2.000 | 100.000 | 3035.600 | 6000.000 |
| 13 | 605.000 | 0.052 | 177.320 | 34.320 | 2.000 | 100.000 | 3302.900 | 6000.000 |
| 14 | 605.000 | 0.052 | 177.320 | 34.320 | 2.000 | 100.000 | 3468.700 | 6000.000 |
| 15 | 605.000 | 0.052 | 177.320 | 34.320 | 2.000 | 100.000 | 3931.000 | 6000.000 |
| ?6 | 605.000 | 0.052 | 177.320 | 34.320 | 2.000 | 100.000 | 4678.000 | 6000.000 |
| 17 | 605.000 | 0.052 | 177.32~ | 34.320 | 2.000 | 100.000 | 5212.000 | 6000.000 |
| 18 | 605.000 | 0.052 | 177.320 | 34.320 | 2.000 | 100.000 | 5406.000 | 6000.000 |

Table A.3: Krypton Performance Data

Krypton.Dat

Mon, Sep 6, •993 11:57 PM

| | Isp (see) | R | Power (kW) | PS (kW) | T (N) | ETA | MASS (kg) | Alpha(kg/kW) | T/? (N/kW) |
|---|---|---|---|---|---|---|---|---|---|
| 1 | 3200.000 | 0.200 | 12.450 | 0.000 | 0.490 | 62.260 | 19.070 | 1.530 | 0.040 |
| 2 | 3600.000 | 0.200 | 21.430 | 0.000 | 0.790 | 65.210 | 21.430 | 1.180 | 0.037 |
| 3 | 4000.000 | 0.200 | 35.050 | 0.000 | 1.210 | 67.500 | 35.050 | 0.940 | 0.034 |
| 4 | 4400.000 | 0.200 | 54.980 | 0.000 | 1.770 | 69.320 | | 0.770 | 0.032 |
| 5 | 4463.000 | 0.200 | 58.820 | 0.000 | 1.870 | 69.560 | 43.910 | 0.750 | 0.032 |
| 6 | 4800.000 | 0.230 | 66.830 | 0.000 | 2.100 | 70.750 | 43.910 | 0.660 | 0.030 |
| 7 | 5200.000 | 0.270 | 77.170 | 0.000 | 2.180 | 71.910 | 43.910 | 0.570 | 0.028 |
| 8 | 5600.000 | 0.310 | 88.340 | 0.000 | 2.340 | 72.860 | 43.910 | 0.500 | 0.027 |
| 9 | 6200.000 | 0.390 | 106.630 | 0.000 | 2.590 | 73.990 | 43.910 | 0.410 | 0.024 |
| 10 | 6600.000 | 0.440 | 119.860 | 0.000 | 2.760 | 74.580 | 43.910 | 0.370 | 0.023 |
| 11 | 7000.000 | 0.490 | 133.920 | 0.000 | 2.930 | 75.100 | 43.910 | 0.330 | 0.022 |
| 12 | 7400.000 | 0.550 | 148.810 | 0.000 | 3.100 | 75.530 | 43.910 | 0.300 | 0.021 |
| 13 | 8000.000 | 0.640 | 172.690 | 0.000 | 3.350 | 76.070 | 38.750 | 0.220 | 0.019 |
| 14 | 8500.000 | 0.720 | 194.010 | 0.000 | 3.560 | 76.430 | 38.750 | 0.200 | 0.018 |
| 15 | 9000.000 | 0.810 | 216.620 | 0.000 | 3.770 | 76.740 | 38.750 | 0.190 | 0.017 |
| 16 | 9470.000 | 0.900 | 239.050 | 0.000 | 3.960 | 77.000 | 38.750 | 0.160 | 0.016 |

| | TS (K) | mdot (g/s) | ID (A) | IB (A) | lg (mm) | Dg (cm) | VB (V) | VT (V) |
|---|---|---|---|---|---|---|---|---|
| 1 | 659.000 | 0.016 | 69.790 | 15.830 | 1.020 | 51.400 | 617.000 | 3084.000 |
| 2 | 656.000 | 0.022 | 99.370 | 22.530 | 1.300 | 65.100 | 781.000 | 3904.000 |
| 3 | 651.000 | 0.031 | 136.310 | 30.910 | 1.600 | 80.340 | 964.000 | 4819.000 |
| 4 | 645.000 | 0.041 | 181.420 | 41.150 | 1.900 | 97.200 | 1166.000 | 5831.000 |
| 5 | 644.000 | 0.043 | 189.330 | 42.900 | 2.000 | 100.000 | 1200.000 | 6000.000 |
| 6 | 640.000 | 0.043 | 189.330 | 42.900 | 2.000 | 100.000 | 1388.000 | 6000.000 |
| 7 | 640.000 | 0.043 | 189.330 | 42.900 | 2.000 | 100.000 | 1629.000 | 6000.000 |
| 8 | 640.000 | 0.043 | 189.330 | 42.900 | 2.000 | 100.000 | 1889.000 | 6000.000 |
| 9 | 640.000 | 0.043 | 189.330 | 42.900 | 2.000 | 100.000 | 2316.000 | 6000.000 |
| 10 | 640.000 | 0.043 | 189.330 | 42.900 | 2.000 | 100.000 | 2624.000 | 6000.000 |
| 11 | 640.000 | 0.043 | 189.330 | 42.900 | 2.000 | 100.000 | 2951.000 | 6000.000 |
| 12 | 640.000 | 0.043 | 189.330 | 42.900 | 2.000 | 100.000 | 3298.000 | 6000.000 |
| 13 | 640.000 | 0.043 | 189.330 | 42.900 | 2.000 | 100.000 | 3855.000 | 6000.000 |
| 14 | 640.030 | 0.043 | 189.330 | 42.900 | 2.000 | 100.000 | 4352.000 | 6000.000 |
| 15 | 640.000 | 0.043 | 189.330 | 42.900 | 2.000 | 100.000 | 4879.000 | 6000.000 |
| ?6 | 640.000 | 0.043 | 189.330 | 42.900 | 2.000 | 100.000 | 5402.000 | 6000.000 |

Table A.4: Argon Performance Data

Argon.Dat · Mon, Sep 6, 1993 11:56 PM

| | Isp (see) | R | Power (kW) | ?s (kW) | T (N) | ETA | MASS (kg) | Alpha(kg/kW) | T / P (N/kW) |
|---|---|---|---|---|---|---|---|---|---|
| 1 | 4100.000 | 0.200 | 17.880 | 0.000 | 0.490 | 55.140 | 18.990 | 1.050 | 0.027 |
| 2 | 4500.000 | 0.200 | 27.430 | 0.000 | 0.710 | 57.240 | 23.640 | 0.860 | 0.026 |
| 3 | 5000.000 | 0.200 | 44.800 | 0.000 | 1.080 | 59.350 | 30.690 | 0.690 | 0.024 |
| 4 | 5500.000 | 0.200 | 70.190 | 0.000 | 1.590 | 61.010 | 39.350 | 0.560 | 0.023 |
| 5 | 5729.000 | 0.200 | 85.170 | 0.000 | 1.870 | 61.660 | 43.910 | 0.520 | 0.022 |
| 6 | 6000.000 | 0.220 | 92.400 | 0.000 | 1.960 | 62.340 | 43.910 | 0.480 | 0.021 |
| 7 | 6500.000 | 0.260 | 106.600 | 0.000 | 2.120 | 63.410 | 43.910 | 0.410 | 0.020 |
| 8 | 7000.000 | 0.300 | 121.940 | 0.000 | 2.280 | 64.290 | 43.910 | 0.360 | 0.019 |
| 9 | 7500.000 | 0.340 | 138.420 | 0.000 | 2.450 | 65.020 | 43.910 | 0.320 | 0.0?8 |
| ?0 | 8000.000 | 0.390 | 156.040 | 0.000 | 2.610 | 65.630 | 43.910 | 0.280 | 0.016 |
| 11 | 8500.000 | 0.440 | 174.790 | 0.000 | 2.770 | 66.130 | 43.910 | 0.250 | 0.0'6 |
| 12 | 9000.000 | 0.490 | 194.680 | 0.000 | 2.940 | 66.570 | 43.910 | 0.230 | 0.015 |
| 13 | 9500.000 | 0.550 | 215.700 | 0.000 | 3.100 | 66.950 | 43..910 | 0.200 | 0.014 |
| 14 | 10000.000 | 0.610 | 237.860 | 0.000 | 3.260 | 67.270 | 38.750 | 0.160 | 0.014 |
| 15 | 10500.000 | 0.670 | 267.160 | 0.000 | 3.430 | 67.550 | 38.750 | 0.150 | 0.013 |
| 16 | 11000.000 | 0.740 | 285.590 | 0.000 | "3.590 | 67.790 | 38.750 | 0.140 | 0.013 |
| 17 | 11500.000 | 0.810 | 311.160 | 0.000 | 3.750 | 68.000 | 38.750 | 0.120 | 0.012 |
| 18 | 12000.000 | 0.880 | 337.870 | 0.000 | 3.910 | 68,190 | 38.750 | 0.110 | 0.011 |
| 19 | 12100.000 | 0.900 | 346.100 | 0.000 | 3.960 | 68.250 | 38.750 | 0.110 | 0.011 |

| | TS (K) | mdot (g/s) | ID (A) | IB (A) | lg (mm) | Dg (cm) | VB (V) | VT (V) |
|---|---|---|---|---|---|---|---|---|
| 1 | 723.500 | 0.012 | 97.110 | 22.790 | 1.020 | 51.200 | 614.000 | 3072.000 |
| 2 | 720.670 | 0.016 | 128.400 | 30.130 | 1.200 | 61.700 | 740.000 | 3701.000 |
| 3 | 715.700 | 0.022 | 176.130 | 41.340 | 1.500 | 76.200 | 914.000 | 4569.000 |
| 4 | 709.690 | 0.029 | 234.430 | 55.020 | 1.800 | 92.100 | 1105.000 | 5529.000 |
| 5 | 706.720 | 0.033 | 264.950 | 62.180 | 2.000 | 100.000 | 1200.000 | 6000.000 |
| 6 | 702.230 | 0.033 | 264.950 | 62.180 | 2.000 | 100.000 | 1316.000 | 6000.000 |
| 7 | 702.230 | 0.033 | 264.950 | 62.180 | 2.000 | 100.000 | 1544.000 | 6000.000 |
| 8 | 702.230 | 0.033 | 264.950 | 62.180 | 2.000 | 100.000 | 1791.000 | 6000.000 |
| 9 | 702.230 | 0.033 | 264.950 | 62.180 | 2.000 | 100.000 | 2056.000 | 6000.000 |
| 10 | 702.230 | 0.033 | 264.950 | 62.180 | 2.000 | 100.000 | 2339.000 | 6000.000 |
| 11 | 702.230 | 0.033 | 264.950 | 62.180 | 2.000 | 100.000 | 2641.000 | 6000.000 |
| 12 | 702.230 | 0.033 | 264.950 | 62.180 | 2.000 | 100.000 | 2960.000 | 6000.000 |
| 13 | 702.230 | 0.033 | 264.950 | 62.180 | 2.000 | 100.000 | 3299.000 | 6000.000 |
| 14 | 702.230 | 0.033 | 264.950 | 62.180 | 2.000 | 100.000 | 3655.000 | 6000.000 |
| 15 | 702.230 | 0.033 | 264.950 | 62.180 | 2.000 | 100.000 | 4030.000 | 6000.000 |
| 16 | 702.230 | 0.033 | 264.950 | 62.180 | 2.000 | 100.000 | 4423.000 | 6000.000 |
| 17 | 702.230 | 0.033 | 264.950 | 62.180 | 2.000 | 100.000 | 4834.000 | 6000.000 |
| 18 | 702.230 | 0.033 | 264.950 | 62.180 | 2.000 | 100.000 | 5264.000 | 6000.000 |
| 19 | 702.230 | 0.033 | 264.950 | 62.180 | 2.000 | 100.000 | 5396.000 | 6000.000 |

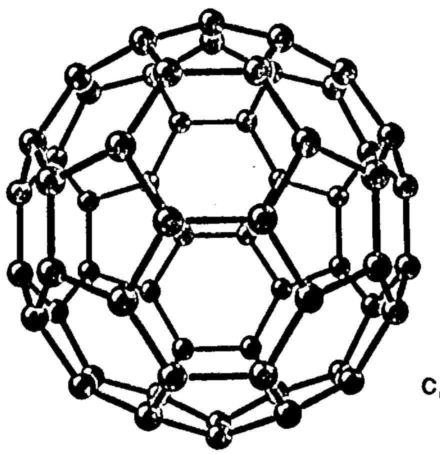

$C_{60}$

Fig 1

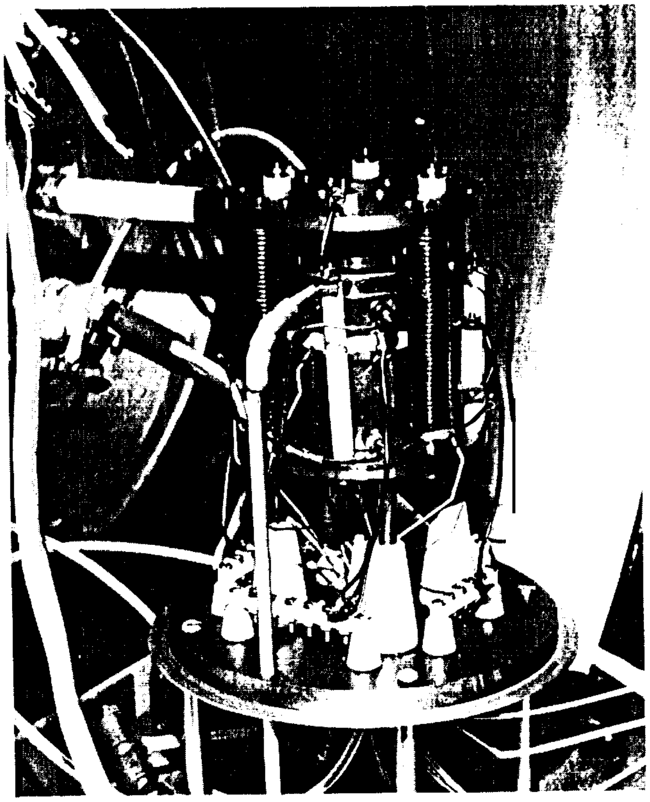

Fig 2

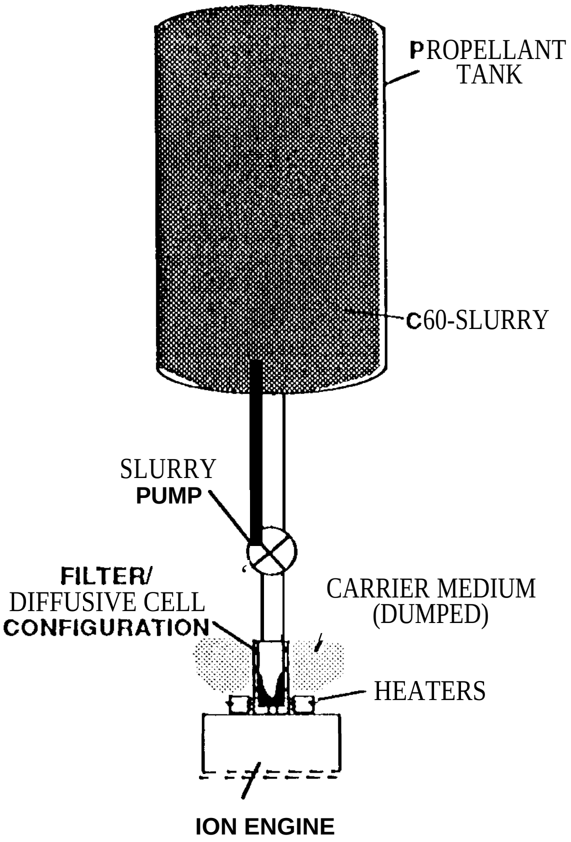
PROPELLANT
TANK
C60-SLURRY
SLURRY
PUMP
FILTER/
DIFFUSIVE CELL
CONFIGURATION
CARRIER MEDIUM
(DUMPED)
HEATERS
ION ENGINE

Fig 3

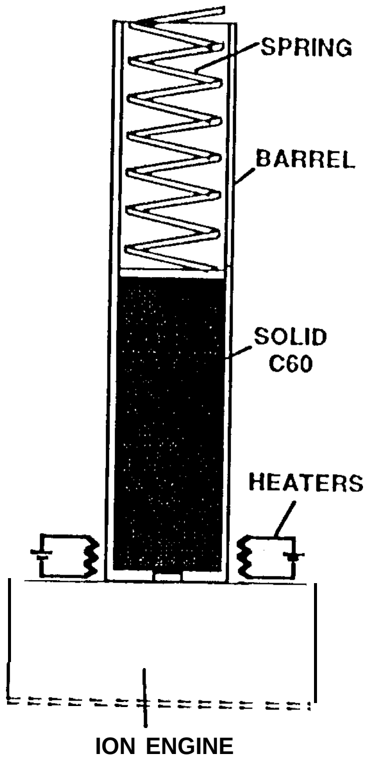


Fig. 4.

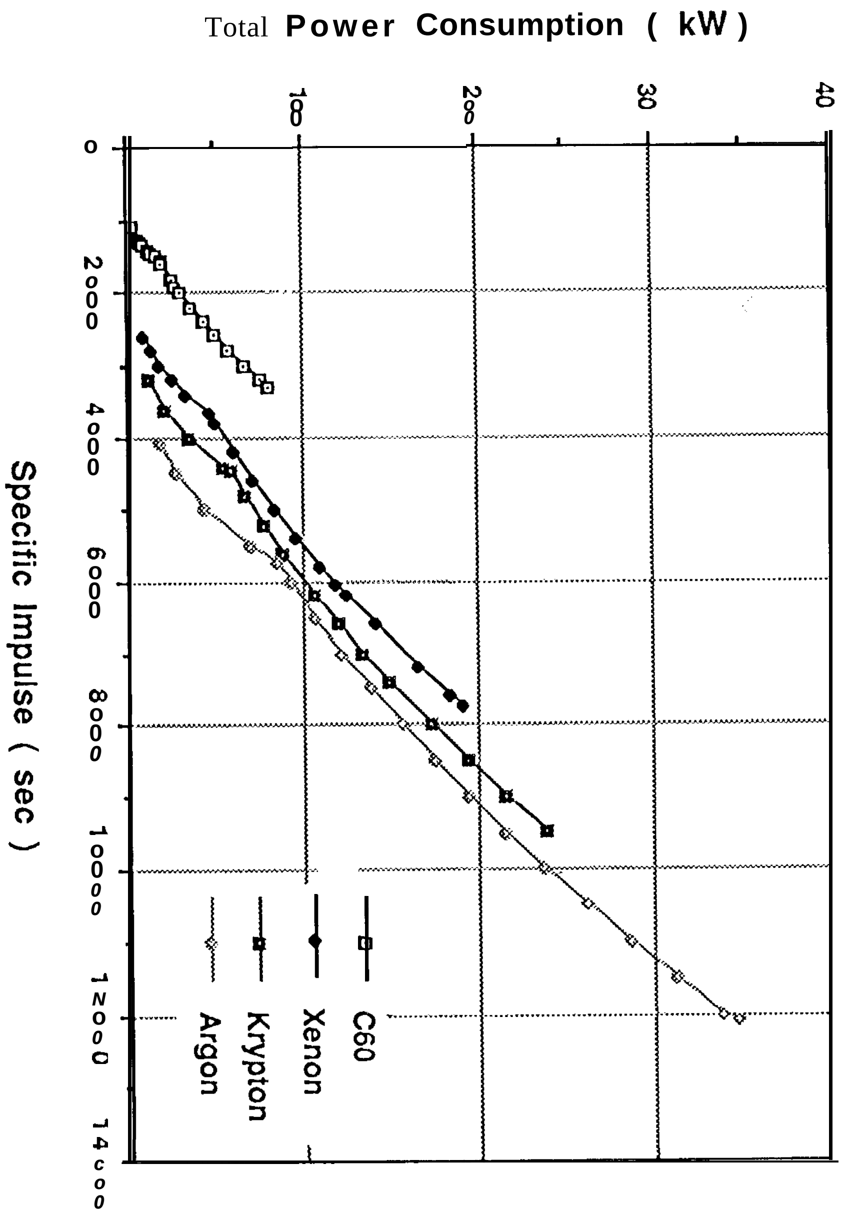
Total Power Consumption ( kW )
0
10
20
30
40
0
2000
4000
6000
8000
10000
12000
14000
Specific Impulse ( sec )
C60
Xenon
Krypton
Argon

Fig. 5

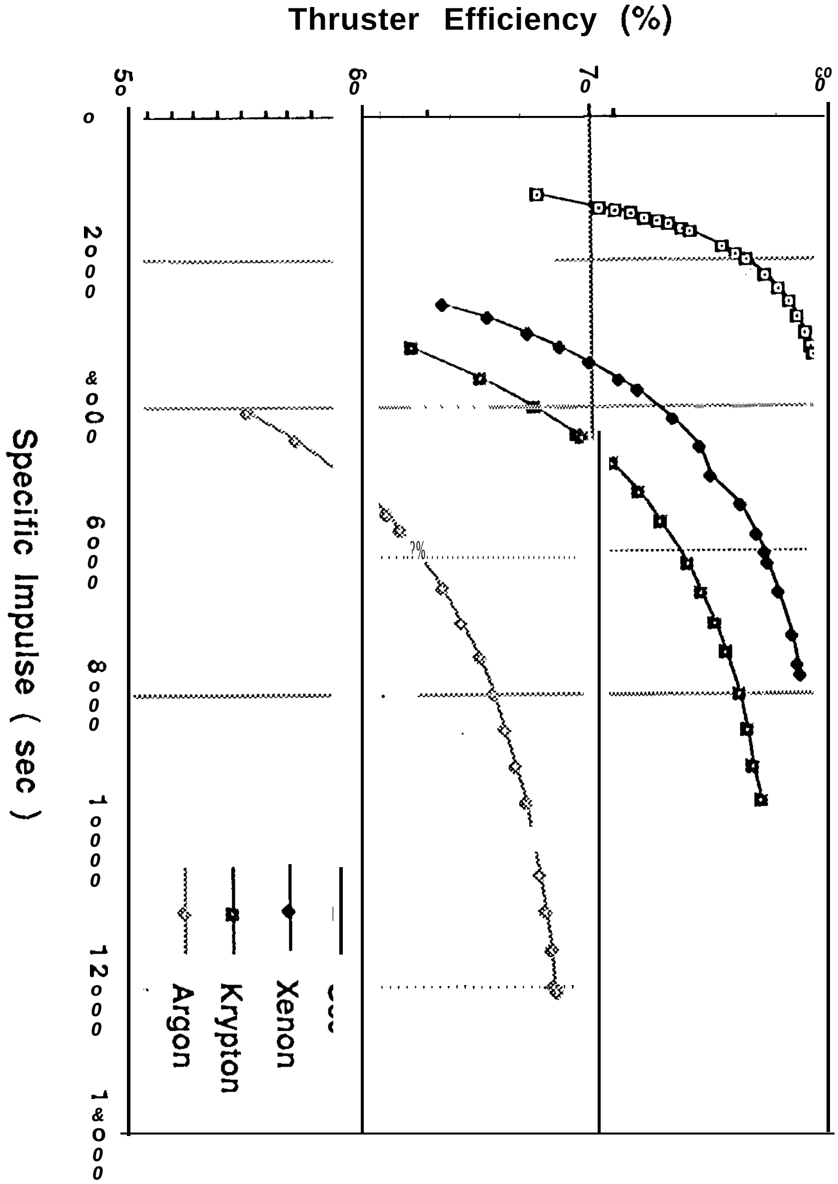
Thruster Efficiency (%)
Specific Impulse ( sec )
Xenon
Krypton
Argon

Fig. 6

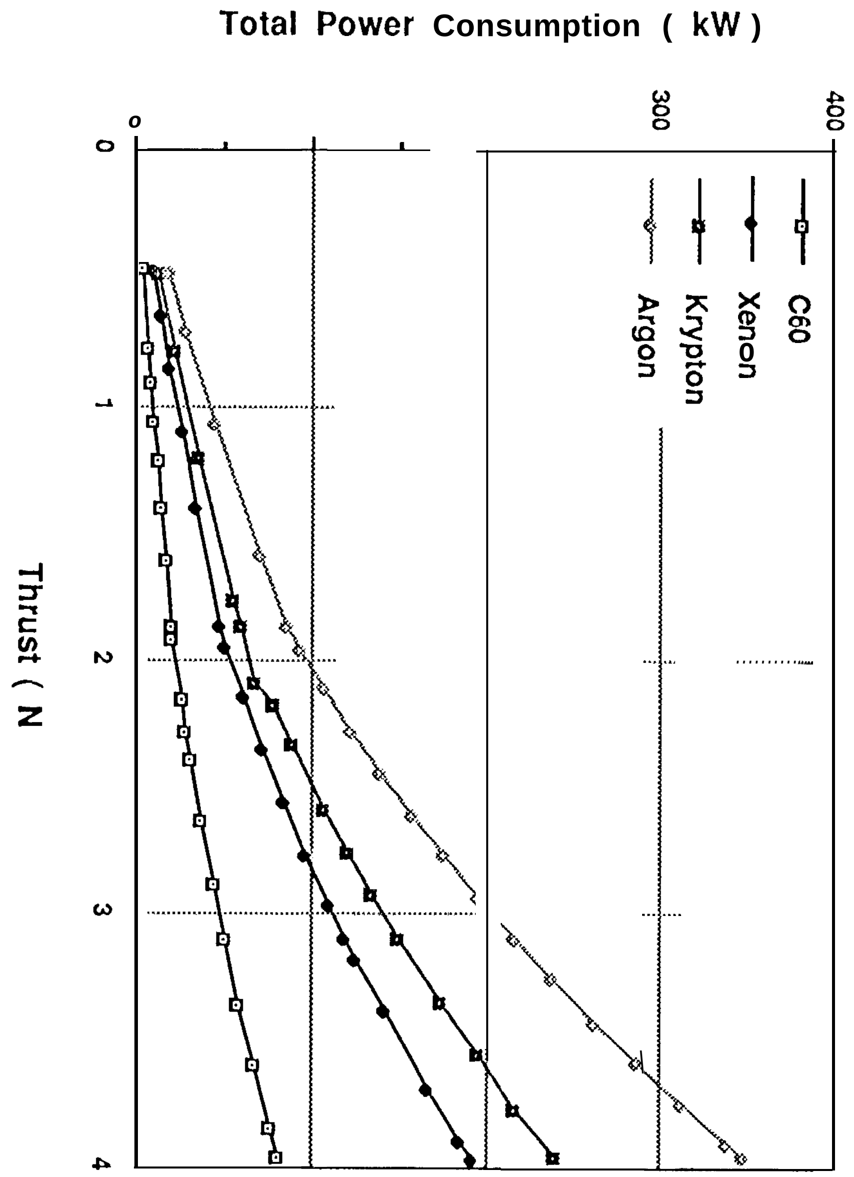
Total Power Consumption ( kW )
400
300
0
C60
Xenon
Krypton
Argon
0
1
2
3
4
Thrust ( N

Fig. 7

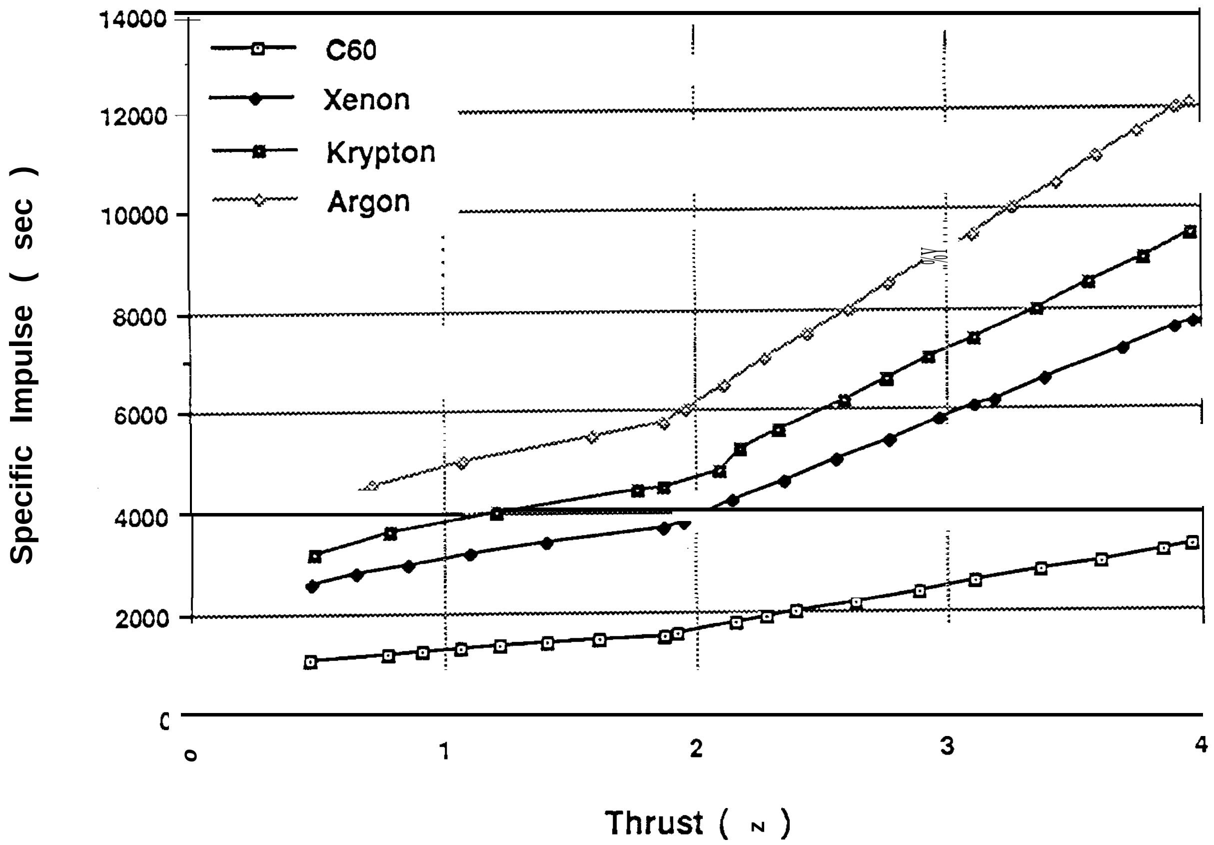
C60
Xenon
Krypton
Argon
Specific Impulse ( sec )
14000
12000
10000
8000
6000
4000
2000
0
1
2
3
4
Thrust ( N )

Fig. 8

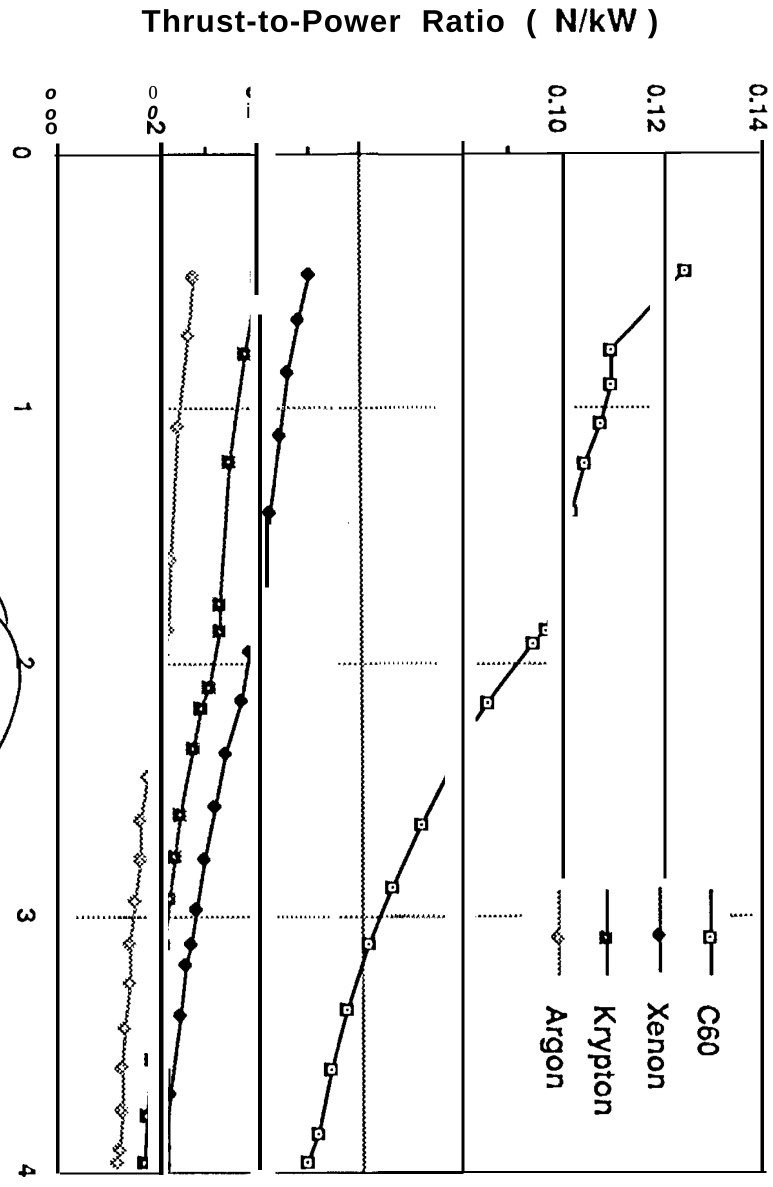


should plot T/P vs Isp

Fig. 9

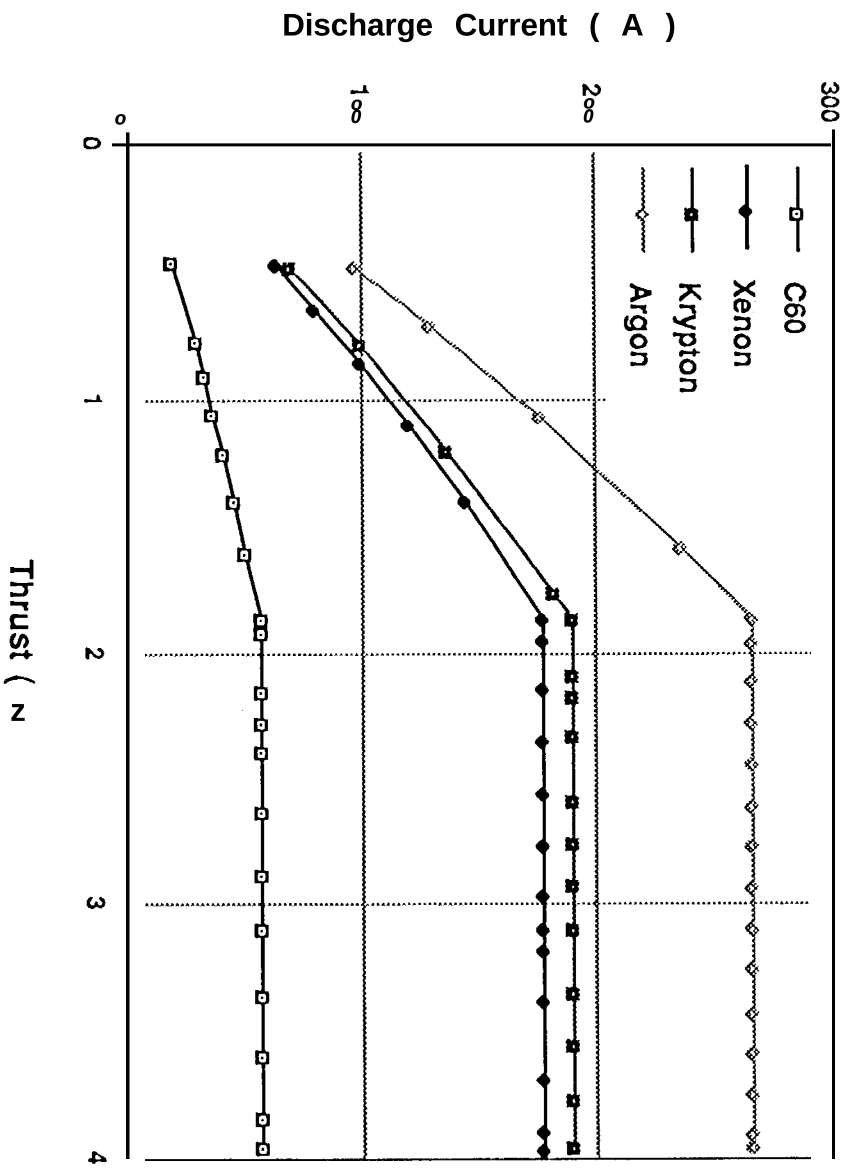
Discharge Current ( A )
0
100
200
300
C60
Xenon
Krypton
Argon
0
1
2
3
4
Thrust ( N

Fig. 10

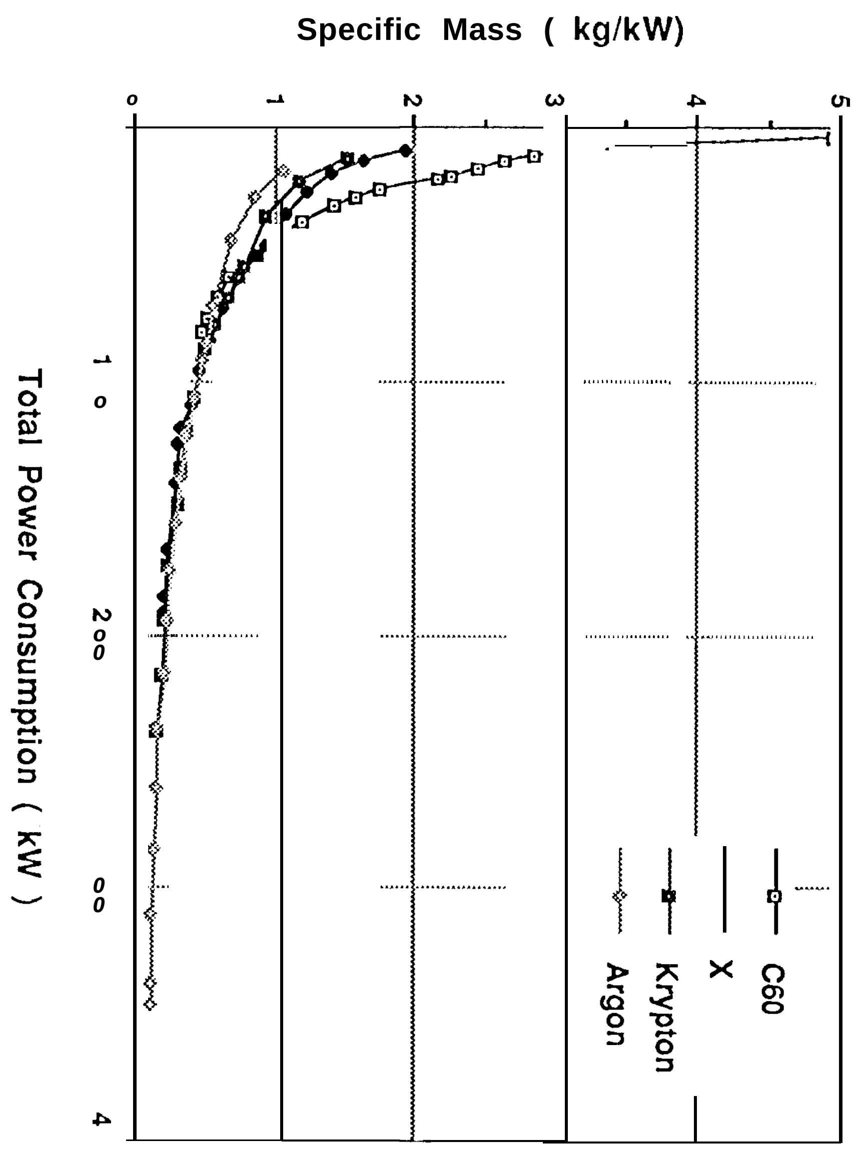

Specific Mass ( kg/kW)
Total Power Consumption ( kW )
C60
X
Krypton
Argon


Fig. 11

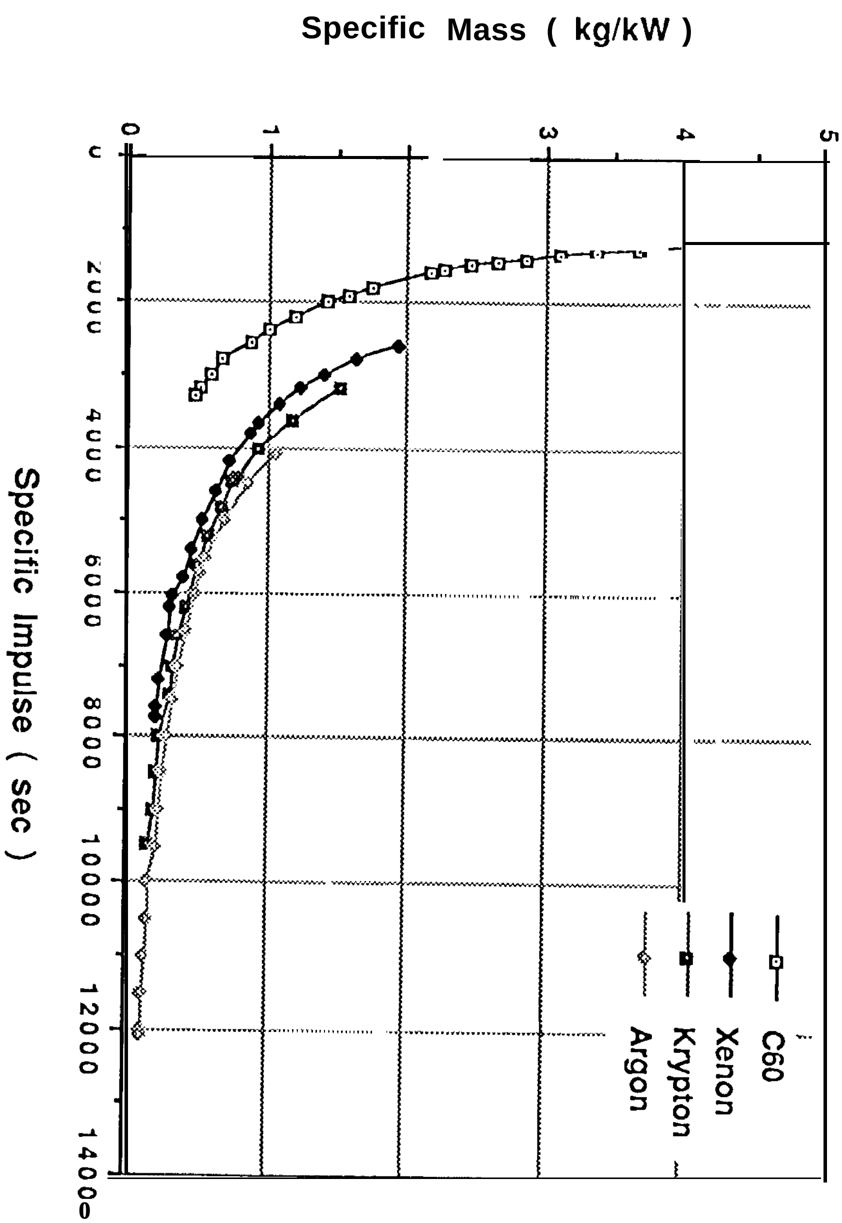
Specific Mass ( kg/kW )
0
1
3
4
5
0
2000
4000
6000
8000
10000
12000
14000
Specific Impulse ( sec )
C60
Xenon
Krypton
Argon

Fig. 12